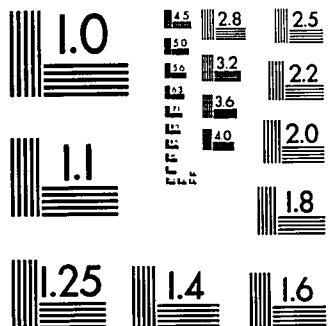
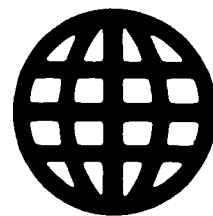


UMI

University Microfilms International



MICROCOPY RESOLUTION TEST CHART
NATIONAL BUREAU OF STANDARDS
STANDARD REFERENCE MATERIAL 1010a
(ANSI and ISO TEST CHART No. 2)

University Microfilms Inc.

300 N. Zeeb Road, Ann Arbor, MI 48106

INFORMATION TO USERS

This reproduction was made from a copy of a manuscript sent to us for publication and microfilming. While the most advanced technology has been used to photograph and reproduce this manuscript, the quality of the reproduction is heavily dependent upon the quality of the material submitted. Pages in any manuscript may have indistinct print. In all cases the best available copy has been filmed.

The following explanation of techniques is provided to help clarify notations which may appear on this reproduction.

1. Manuscripts may not always be complete. When it is not possible to obtain missing pages, a note appears to indicate this.
2. When copyrighted materials are removed from the manuscript, a note appears to indicate this.
3. Oversize materials (maps, drawings, and charts) are photographed by sectioning the original, beginning at the upper left hand corner and continuing from left to right in equal sections with small overlaps. Each oversize page is also filmed as one exposure and is available, for an additional charge, as a standard 35mm slide or in black and white paper format.*
4. Most photographs reproduce acceptably on positive microfilm or microfiche but lack clarity on xerographic copies made from the microfilm. For an additional charge, all photographs are available in black and white standard 35mm slide format.*

***For more information about black and white slides or enlarged paper reproductions, please contact the Dissertations Customer Services Department.**

UMI University
Microfilms
International

8601144

Irani, Fersheed K.

**A COMPREHENSIVE EXPERIMENTAL STUDY OF THE FRACTURE BEHAVIOR
OF GRANITE UNDER THREE DIMENSIONAL LOADING, AT AMBIENT
TEMPERATURE AND 300 DEGREES FAHRENHEIT**

The University of Oklahoma

Ph.D. 1985

**University
Microfilms
International** 300 N. Zeeb Road, Ann Arbor, MI 48106

THE UNIVERSITY OF OKLAHOMA
GRADUATE COLLEGE

A COMPREHENSIVE EXPERIMENTAL STUDY OF THE
FRACTURE BEHAVIOR OF GRANITE UNDER
THREE DIMENSIONAL LOADING, AT
AMBIENT TEMPERATURE AND 300° F.

A DISSERTATION
SUBMITTED TO THE GRADUATE FACULTY
in partial fulfillment of the requirements for the
degree of
DOCTOR OF PHILOSOPHY

BY
FERSHEED K. IRANI
NORMAN, OKLAHOMA
1985

A COMPREHENSIVE EXPERIMENTAL STUDY OF THE FRACTURE
BEHAVIOR OF GRANITE UNDER THREE DIMENSIONAL
LOADING, AT AMBIENT TEMPERATURE AND 300° F.

A DISSERTATION

APPROVED FOR THE SCHOOL OF
AEROSPACE, MECHANICAL AND NUCLEAR ENGINEERING

By

Achut S. Kha

Charles W. Beitz

John P. D'Almeida

David M. Eagle

Kenneth V. Ruffa

ACKNOWLEDGMENTS

It is impossible of course to properly express the gratitude that is felt towards the individuals that have contributed to the completion of this work. To the few mentioned here and the many who are not, I am sincerely grateful.

Dr. Akhtar S. Khan, for his continued encouragement and valuable guidance throughout this study and my entire graduate degree program. The excellence and high professional standards exemplified by him as a teacher and advisor will have a favorable and lasting influence upon my professional career. It is with a deep sense of gratitude that I acknowledge the opportunity I had to study and work under his guidance. My gratitude to Dr. D. M. Egle, Dr. Wm. R. Upthegrove, Dr. C. W. Bert and Dr. K. V. Luza for serving on my dissertation committee, and, to Dr. J. Wickham and Dr. D. Sterns for their valuable suggestions and guidance.

Appreciation is extended to Oklahoma Mining and Mineral Resources Research Institute for their fellowship during my tenure as a graduate student, and to Mr. Bob Arndt, Director, OMMRRI for his continued support, interest and guidance in the completion of this effort.

Special thanks to William Petre for his accurate machining and the technical staff of the AMNE department and Mark Meredith of Petroleum Engineering department for their technical assistance and support. Thanks also to Mr. K. Y. Liu for the design of the pressure vessel.

A special thanks to Ms. Lynn Crussel for her patience in typing this manuscript.

Finally, it has been my family who have sacrificed the most. The author wishes to express his great admiration for his dear wife, Dilzi, for several years of unwavering kindness, love, support and encouragement. My son, Justin, for just being there and to my parents and in-laws for giving a helping hand. Without their encouragement and support there would have been little reason for its completion.

Fersheed K. Irani

ABSTRACT

This study presents the results of the triaxial loading experiments performed to determine the fracture strength characteristics of granite subjected to truly three dimensional loading. These measurements were carried out on thin walled hollow cores which were subjected to various tension-torsion, compression-torsion loading paths, in the presence of confining pressures of up to 7000 psi, at ambient temperature and at 300° F. These results are compared with the classical failure theories of Coulomb-Mohr and Drucker and Prager. It is observed that none of the above criteria are able to predict the failure over the entire range of stresses, and at different temperatures. A new failure criterion based on the strain energy density and first stress invariant (J_1) is proposed, to predict the failure envelope over the entire range of stresses and at different temperatures. Firstly, the results of the work done by three independent investigators on the failure of granite are compared with the Coulomb-Mohr, Drucker and Prager and the proposed new criterion. The improved effectiveness of the proposed new criterion in predicting the failure of granite relative to the other two criteria is then demonstrated. Also, failure results of four other commonly studied rocks (Solenhofen Limestone, sandstone, marble, and shale) are compared with the Coulomb-Mohr, Drucker and Prager, and the proposed new criterion. The improved or equal effectiveness of the proposed new criterion in predicting the failure of these common rocks relative to the other two criteria is also demonstrated.

TABLE OF CONTENTS

	Page
ABSTRACT	iii
LIST OF TABLES	v
LIST OF ILLUSTRATIONS	vi
CHAPTER	
I. INTRODUCTION	1
II. EXPERIMENTAL PROCEDURE	7
III. THEORETICAL ANALYSIS	16
IV. EXPERIMENTAL RESULTS AND DISCUSSION	21
V. SUMMARY AND CONCLUSIONS	64
REFERENCES	66
APPENDIX	70

LIST OF TABLES

	Page
1. Stress components at failure for various tests at ambient temperature	23
2. Principal stresses, J_1 , $(J_2d)^{1/2}$, U_0 at failure for various test at ambient temperature	25
3. Stress components at failure for various tests at 300° F	39
4. Principal stresses, J_1 , $(J_2d)^{1/2}$, U_0 at failure for various tests at 300° F	40
5. Experimental data of Wong (46), for Westerly Granite	71
6. Experimental data of Brace (45) for granite	72
7. Experimental data of Smith et al. (21) for granite	73
8. Experimental data of Smith et al. (21) for sandstone	74
9. Experimental data of Smith et al. (21) for marble	75
10. Experimental data of Smith et al. (21) for shale	76
11. Experimental data of Green et al. (18) for Solenhofen Limestone	77
12. Experimental data of Handin et al. (36) for Solenhofen Limestone	78

LIST OF FIGURES

	Page
1a. Schematic diagram of the tension-torsion machine (front view)	8
1b. Schematic diagram of the tension-torsion machine (side view)	9
2. Sectional view of the high pressure vessel cylinder assembly	10
3a. Schematic diagram of the tension-torsion machine with the pressure vessel assembly (front view)	11
3b. Schematic diagram of the tension-torsion machine with the pressure vessel assembly (side view)	12
4. Schematic diagram of the external pressure test	15
5. Coulomb-Mohr criterion	17
6. Drucker and Prager criterion	17
7a. Element in state of pure shear	19
7b. Mohr's stress circle for pure shear	19
7c. Element oriented with its faces parallel to the principal plane	19
8. Coordinate system	22
9. Uniaxial tensile stress-strain curve for granite at ambient temperature	27
10. Shear stress-strain curve for granite at ambient temperature	28
11. Uniaxial compressive stress-strain curve for granite at ambient temperature	29
12. Equivalent stress-strain curve for granite under combined loading at ambient temperature	30
13. A plot of $\frac{\sigma_1 - \sigma_3}{2}$ versus $\frac{\sigma_1 + \sigma_3}{2}$ for various tests at ambient temperature	32
14. A plot of $(J_2d)^{1/2}$ versus J_1 for various tests at ambient temperature	33

LIST OF FIGURES (CONTINUED)

	Page
15. A plot of U_0 versus J_1 for various tests at ambient temperature	36
16. A plot of U_0 versus J_1 showing the external pressure test results at ambient temperature	37
17. Uniaxial tensile stress-strain curve for granite at 300° F . .	41
18. Shear stress-shear strain plot for granite at 300° F	42
19. Uniaxial compressive stress-strain curve for granite at 300° F	43
20. A plot of $\frac{\sigma_1 - \sigma_3}{2}$ versus $\frac{\sigma_1 + \sigma_3}{2}$ for various tests at 300° F .	45
21. A plot of $(J_{2d})^{1/2}$ versus J_1 for various tests at 300° F . . .	46
22. A plot of U_0 versus J_1 for various tests at 300° F	48
23. A plot of U_0 versus J_1 , showing the results of the external pressure test at 300° F	49
24. A plot of U_0 versus J_1 for all the tests on granite at ambient temperature and at 300° F	50
25. A plot of U_0 versus J_1 , showing the results of the external pressure test results at ambient temperature and at 300° F	51
26. A plot of $\frac{\sigma_1 - \sigma_3}{2}$ versus $\frac{\sigma_1 + \sigma_3}{2}$ for the results of Wong, Smith et al., and Brace et al.	53
27. A plot of $(J_{2d})^{1/2}$ versus J_1 for the results of Wong, Smith et al., and Brace et al.	54
28. A plot of U_0 versus J_1 for the results of Wong, Smith et al., and Brace et al.	55
29. A plot of $\frac{\sigma_1 - \sigma_3}{2}$ versus $\frac{\sigma_1 + \sigma_3}{2}$ for Solenhofen Limestone . .	58
30. A plot of $(J_{2d})^{1/2}$ versus J_1 for Solenhofen Limestone	59
31. A plot of U_0 versus J_1 for Solenhofen Limestone	60

LIST OF FIGURES (CONTINUED)

	Page
32. A plot of $\frac{\sigma_1 - \sigma_3}{2}$ versus $\frac{\sigma_1 + \sigma_3}{2}$ for sandstone, shale and marble	61
33. A plot of $(J_{2d})^{1/2}$ versus J_1 for sandstone, shale and marble.	62
34. A plot of U_0 versus J_1 for sandstone, shale and marble . . .	63

I. INTRODUCTION

Studies on the deformation and fracture of rocks under combined stresses have been of interest to researchers since the early work of Adams (1-4). At the turn of the century, Adams and Nicholson⁽¹⁾ demonstrated that rocks change their character when a confining pressure is applied, so that they are no longer brittle but behave plastically. This was done by subjecting the rock samples to uniaxial compression, the rock itself was constrained in the radial direction by a steel jacket. His apparatus had inherent defects, however, which made it impossible for him to get more than qualitative measurements of the forces necessary to cause deformation and the strength under confining pressure. The first triaxial compression tests in which a truly measurable hydrostatic confining pressure was applied to the specimen were those of von Karman (5) who deformed cylindrical specimens of Carrara Marble and red sandstone under pressure of several thousand atmospheres. This has been followed by the work of Bridgman (6) who studied the strength of rocks under low to very high confining pressure, in compression and in shear.

Griggs (7-10) was the first investigator to overcome the defects present in Adams' experimental technique by developing confining pressure surrounding the specimen using a liquid of fairly low viscosity. His studies gave values for strength and change in mode of fracture and they permitted the study of plasticity in specimens caused by confining pressure. He was also the first investigator to carry out triaxial compression tests at elevated temperatures.

Since the pioneering work of Adams and Nicholson, as well as von Karman and Griggs, excellent data on the effects of hydrostatic pressure and temperature upon rock strength and deformation characteristics have been reported. An extensive bibliography on the subject can be found in reference (12).

Geologists developed an interest in the plastic flow and fracturing of rocks in the mid-thirties. Leith and Sharpe (13) explained that fracturing of rocks will result when stresses are built up more rapidly than the material can reorganize itself by recrystallization. Later Griggs (9) reported experimental data contradictory to this hypothesis. He observed that the amount of plastic deformation decreases as the duration of experiment is increased for specimen compressed under conditions of similar temperatures and confining pressures, but with different rates of increase of differential pressure.

Triaxial compression tests on Solenhofen limestone subjected to 2,000 atmospheres and at room temperature were carried out by Robertson (14). He investigated the elastic limit as a function of strain rate, and reported the effects of hydrostatic pressure and temperature on the plastic deformation of rocks. He also examined the experimental data with respect to various failure criteria. Similar triaxial studies were later carried out by various investigators (15-23) at different temperatures and various strain rates on a variety of rocks. The specimens used in these tests were either solid and/or hollow cores. Goldsmith (25) studied the stress-strain curve and the fracture strength of Barre Granite using the split Hopkinson bar technique.

An effective stress law for elastic strain of aggregates with pore pressure was proposed by Nur (26). The expression he derived has its limitation in that it can be applied for only elastic strains and the law is not applicable to inelastic processes such as frictional sliding and fracture. Barla (27) attempted to develop the constitutive equations for rocks with respect to simulation of three material behavior patterns, linearly elastic, nonlinearly elastic and time dependent.

A three-part equation to relate volumetric strain to axial stress in compression was proposed by Bordia (28). He also developed an equation for

Poisson's ratio in the microcracking region. Hudson et al. (29) studied the shape of the complete stress-strain curve with particular emphasis on the rock specimen geometry. Fourteen physical properties of rocks were corelated using a statistical approach method by Judd and Hubner (30). They reported a direct linear relationship between modulus of rigidity and Young's modulus, between compressive strength and Young's modulus, and between laboratory values of the static and dynamic moduli of elasticity.

An extensive investigation on the tensile strength of laminated rocks was carried out by Hobbs (32). Hardy (33) carried out experiments to study the failure of Indiana limestone under combined stress state. In his experiments, hollow cylindrical rock specimens were loaded simultaneously under axial tensile loads and internal pressure. Yield and initial failure were detected using acoustic emission techniques. The effects of combined stresses on the fracture strength of two rocket nozzle grade graphites was studied by Ely (34). He carried out experiments at room temperature and a biaxial stress state was created by internal pressure and axial loads. Few investigators have reported the effects of intermediate principal stress on the failure of rocks. Handin et al. (36) are some of them. They undertook the study of the intermediate principal stress on the failure of limestone, dolomite, and glass at temperatures in the range of 25 to 500°C, confining pressure of 10 kb. and strain rates ranging from 10^{-4} to 10^{-7} per second. They used solid as well as hollow cylinders in their experiments. Failure and post failure of Westerly Granite were studied by Wong (46) at pressures of up to 400 MPa and temperatures up to 700°C. He reported that at pressures above 80 MPa, crack morphology changes induced by thermal cracking have no significant effect on fracture strength, and the loading history plays a significant role in the post failure behavior of Westerly Granite.

A theoretical and experimental analysis of a change in volume of a porous medium due to change in external and internal pressures has been reported by Van Der Knaap (38) and Brace et al. (45). Russell and Hoskins (50) investigated the problem of residual stresses in rocks and concluded that the size of strain gage relative to the grain size is probably an important factor in such a study. Cristescu (39) has worked on the problem of rock plasticity and the various effects of time on its properties. He has also proposed viscoelastic constitutive equations to describe such rock behavior. Recently Kim and Lade (40) have developed a criterion to describe three dimensional failure of rocks. The criterion they proposed was formulated in terms of the first and the third stress invariants and it also involves three independent material parameters. They have also proposed an expression for the evaluation of uniaxial tensile strength on the basis of uniaxial compressive strength.

The above literature review reveals that the most widely used method to study and understand the behavior and failure of rocks has been "three dimensional compression" and "three dimensional tension" techniques where the solid cylindrical cores are loaded in uniaxial compression in the presence of confining pressure. If this compression is less than the confining pressure, then it is assumed to give a "three dimensional tensile" loading. However, in both these cases, all three principal stresses are compressive in nature. Also in torsion tests carried out on solid cores, the shear stresses are not uniform through the thickness; they are functions of the radius at any point on the core.

In most of the previous studies, the strains were calculated by measuring displacements of the ends of the core in the axial and radial directions. This technique of measuring strains is not accurate, especially for small strains. These loading and strain measuring techniques, although widely used,

definitely have limitations. Also, in order to understand the true behavior and failure of rocks which are bimodular (different Young's modulus in tension and compression) it is necessary that these different properties in tension and compression are incorporated in developing the failure criterion. Very little or no importance has been given to such rock behavior in the past.

In this present study, an in-depth experimental investigation of the behavior and failure of granite at ambient temperature and at 300°F, under truly three dimensional loading conditions is undertaken. This is accomplished by designing and developing an experimental apparatus which has the capability of applying truly three dimensional loading on hollow rock cores. The strains in the rock specimen are accurately measured by bonded strain gage rosettes on the surface of the core. Numerous experiments are carried out by subjecting hollow rock specimens to various loading paths such as tension, compression, torsion, combinations of tension-torsion loading, combinations of compression-torsion loading at atmospheric pressure and under confining pressures of up to 7000 psi to obtain one, two and three dimensional loading situations. These experiments were carried out at both the ambient temperature and at a temperature of 300°F to understand and study the the behavior and failure of rocks under truly three-dimensional loading conditions, and the effects of temperature on such behavior. All the above experiments were carried out on thin walled hollow cylinders cored from granite (sienna pink) rock, obtained from the Roosevelt Granite Company quarry, west of Snyder, Oklahoma, (SE SE NW 5 Sec. T.2N.,R.17W.). The choice of this particular granite was made because of its homogeneity, uniform grain size, high strength, and availability.

The experimental results obtained from these tests are then compared with the existing failure criteria of Tresca, Coulomb-Mohr, Von Mises, and Drucker

and Prager. It is then shown that none of these failure criteria are able to predict the fracture behavior over the entire range of stresses and at different temperatures. A new failure criterion in terms of strain energy density and the first stress invariant is proposed. The validity of this proposed criterion is then demonstrated over the entire range of stresses at failure and also at different temperatures. The proposed new criterion along with the criteria of Coulomb-Mohr and Drucker and Prager, are compared with the experimental results of three other independent investigators on the failure of granite and other four commonly studied rocks (Solenhofen Limestone, sandstone, marble and shale). The improved effectiveness of the proposed new criterion in predicting the failure of rocks over the other two criterion is then demonstrated.

II. EXPERIMENTAL PROCEDURE

Hollow cylindrical rock specimens are obtained by coring twice, first with a core drill of 1.25 inches (31.75 mm) diameter and then with a core drill of 1.875 inches (47.6 mm) diameter. This results into a hollow cylindrical specimen with outer diameter of 1.68 inches (42.6 mm) and inner diameter of 1.25 inches (31.75 mm). Two different assembly procedures are then followed in order to mount the hollow rock specimen on the loading apparatus, depending on whether a two dimensional or a three dimensional loading experiment is to be carried out.

In case of two dimensional loading experiments, the rock specimen is first bonded to the upper and lower grips G_U and G_L respectively by means of high-strength epoxy. This subassembly is then mounted on the experimental apparatus as shown in Figure 1. In case of three dimensional loading experiments, the rock specimen is first bonded between the grips, G_U at the upper end, and G_L at the lower end by means of high-strength epoxy, in a specially designed assembly fixture which ensures that the specimen axis coincides with the axis of the grips and the axis of the pressure vessel which is also the axial loading axis. This subassembly is then assembled with the high-pressure cylinder and the cylinder end caps using proper size o-rings and rubber gaskets between end caps and the cylinder (see Figure 2). The complete pressure vessel assembly is then mounted to the testing machine, Fig. 3. The testing machine is a dead weight type tension-torsion machine in which the loading, unloading, and reloading is applied at a constant stress rate.

The upper grip is attached to a 4.5 inches (114.3 mm) diameter drum 'D' and forced tangentially to the drum to apply torque to the specimen. The upper grip is free to rotate about its axis while such rotation of the lower grip is prevented. The lower grip is free to rotate about the other two axes

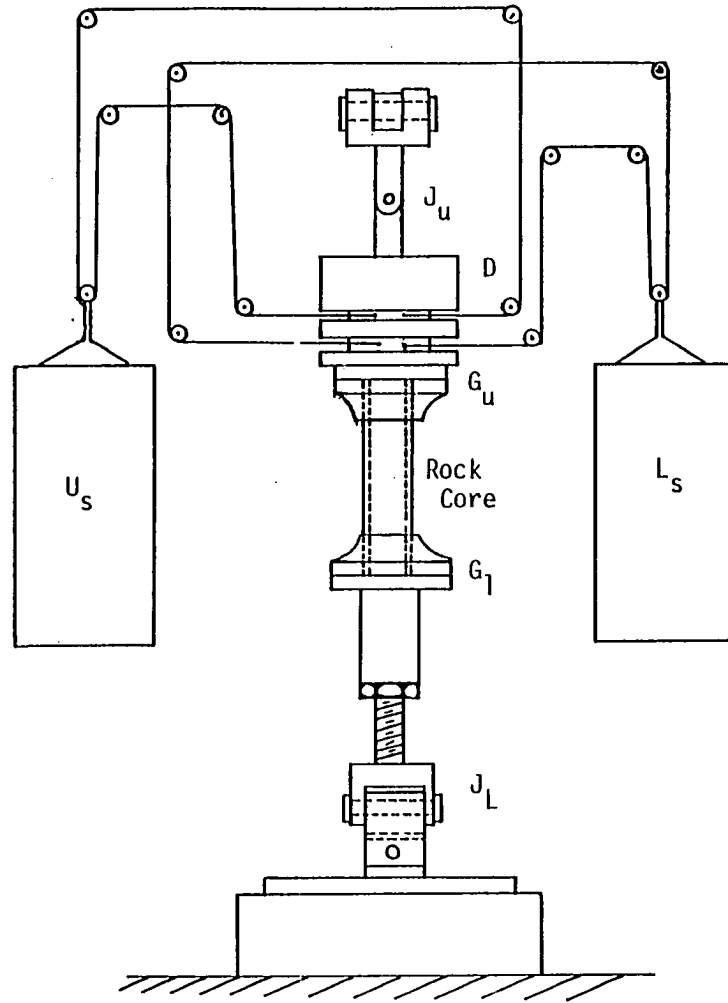


Figure 1a. Schematic diagram of the tension-torsion machine (front view).

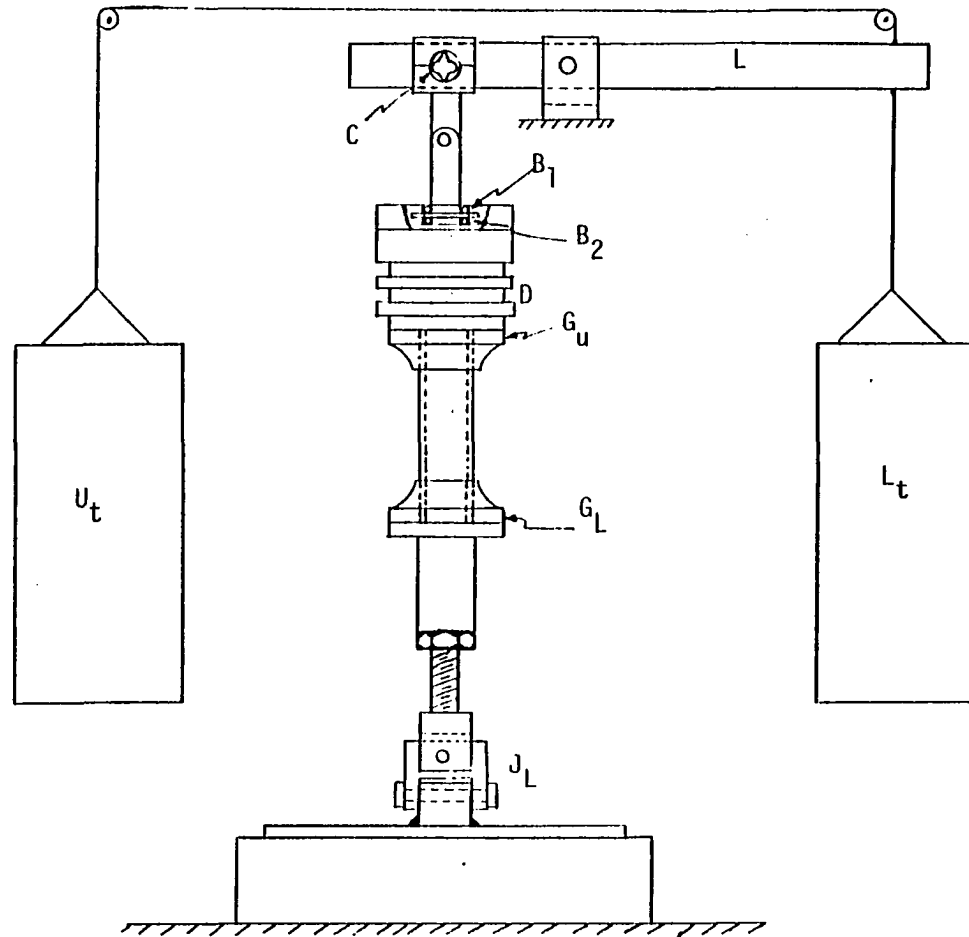


Figure 1b. Schematic diagram of the tension-torsion machine (side view).

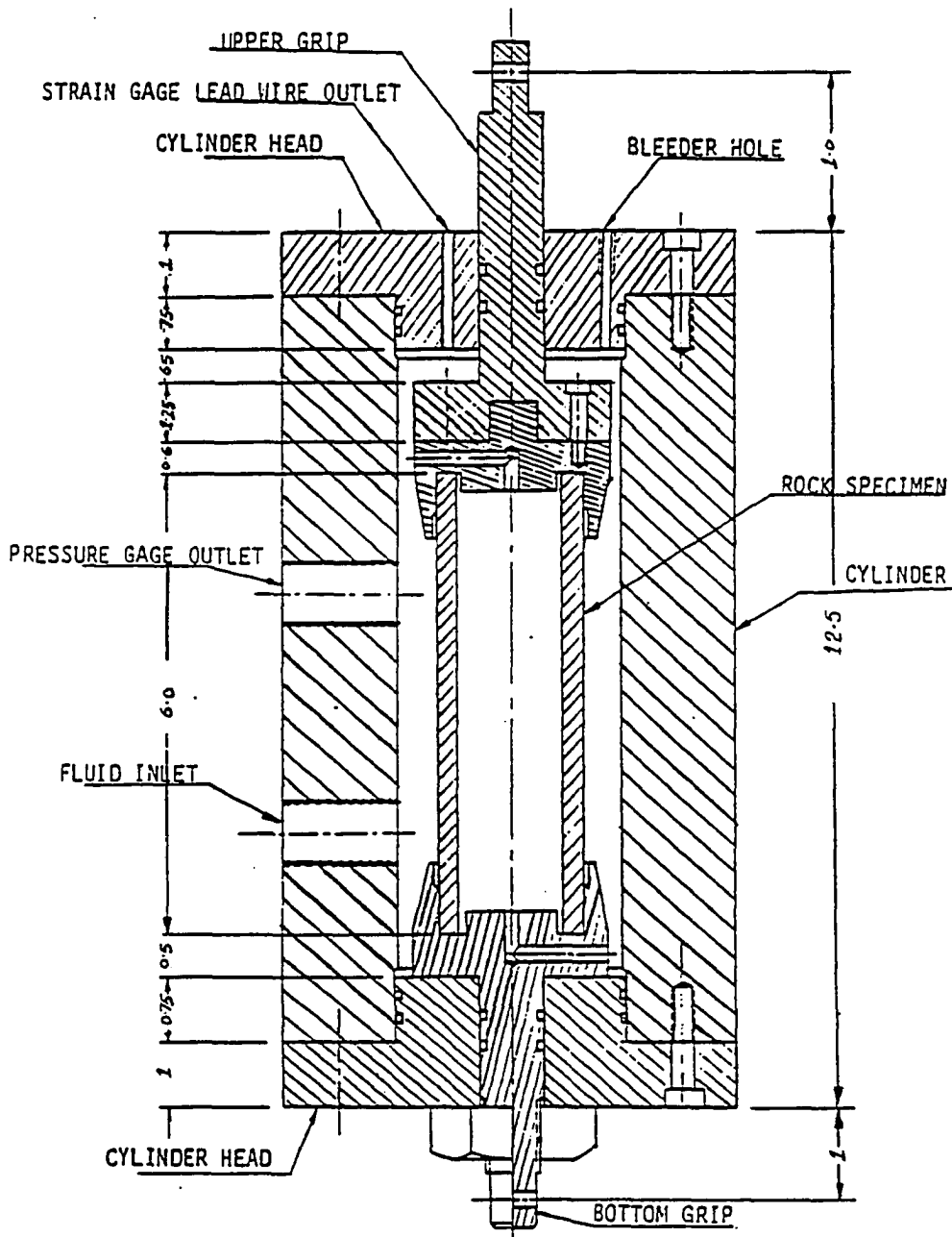


Figure 2. Sectional view of the high pressure vessel cylinder assembly. All dimensions in inches.

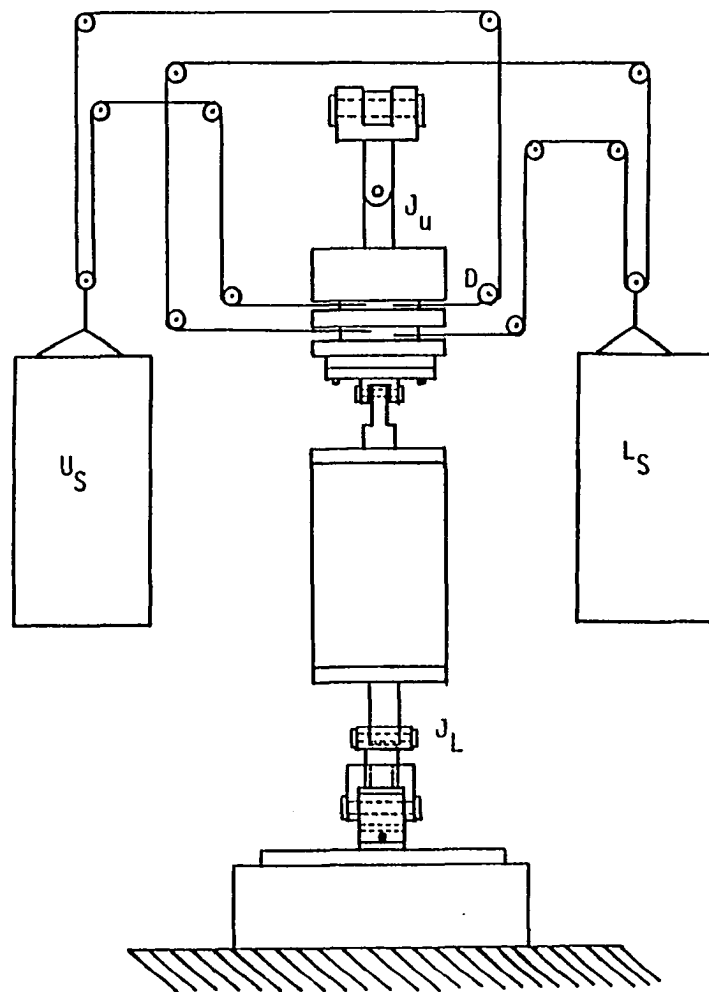


Figure 3a. Schematic diagram of the tension-torsion machine with pressure vessel assembly (front view).

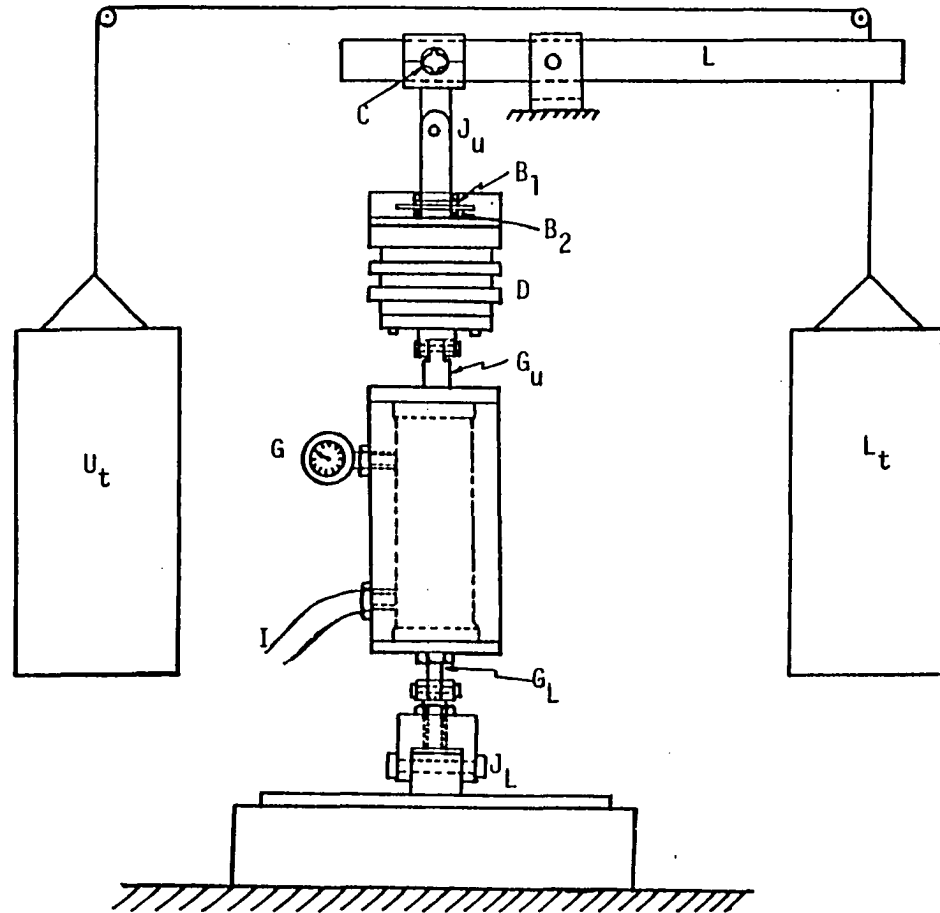


Figure 3b. Schematic diagram of the tension-torsion machine with pressure vessel assembly (side view)

perpendicular to the axial direction at G_L . Its alignment in the vertical plane is ensured by universal joints J_U and J_L at the upper and the lower ends respectively. Tangential forces on the drum, which is connected to the upper grip, is achieved by means of aircraft steel cable connected to the loading bucket L_S through symmetrically located low-friction pulleys. Unloading is achieved through an unloading bucket U_S , which causes tangential forces in the opposite direction.

The specimen is subjected to tensile or compressive loading through barrel L_t or U_t respectively, lever arm 'L', dual knife edge cam 'C', and universal joint J_U . The universal joint J_U is connected to the drum through thrust bearings B_1 and B_2 so that the two combinations of loads (tension-torsion or compression-torsion) can be applied independently of each other. In case of both tension/compression and torsion, the loading as well as the unloading is achieved by water flowing under a constant head from an overhead tank. The rate of loading and unloading can be controlled by changing the outlet nozzle; a larger inside diameter of the outlet nozzle results in a higher stress rate.

Hydrostatic pressure in the range of 0-15,000 psi can be developed surrounding the core using a Haskell AW-150 air amplifier pump and 10W-40 oil as the fluid medium. The specimen is insulated from both inside and outside by coating it with a thin layer of commercially available silicone rubber paste and allowing it to cure for 24 hours. The pressure gage 'G' measures the fluid pressure inside the pressure chamber. The desired pressure in the pressure chamber is controlled by regulating the inlet air pressure to the air amplifier pump. A constant inlet air pressure of 'p' maintains a constant fluid pressure of "150 p" in the pressure chamber.

The strains in the rock sample are measured by electrical resistance

metallic-foil strain gages bonded on the outside and inside surfaces of the core. Micro-Measurements cement type M-Bond 200 (or Eastman 910) is used to mount the strain gages on the rock sample, for ambient temperature tests. For experiments at 300° F, Micro-Measurements M-Bond 600 adhesive is used to bond the strain gage on the rock sample with the recommended curing procedure. Two different kinds of gages, manufactured by Kyowa, will be used. The first type (KDF-5-C1-11) is a general purpose constantin alloy foil gage with polyimide backing of gage length 5 mm and a resistance of 120 ohms. The other type (KFC-10-D17-11) is a specially designed for concrete. The strains are measured and recorded using a Vishay switch and balance unit (Model #SD-1) and strain indicator (Model #P-3500) manufactured by Measurements Group.

Experiments at the high temperature of 300°F were carried out by heating the pressure vessel externally using Fisher Scientific Company heavy insulated heating tape (Cat No. 11-463-51D) which is suitable for direct contact with metals. The temperature of the rock specimen was monitored by mounting a J-type thermocouple on its surface and the temperature was controlled using a temperature controller manufactured by OMEGA Engineering Inc. (Model 4001). In all the experiments at high temperature, white mineral oil was used as a confining fluid. In the external pressure test experiments (Figure 4), hollow rock cores with closed ends were subjected to external pressure until failure, and the average stresses in the rock were calculated using thick-wall cylinder equations.

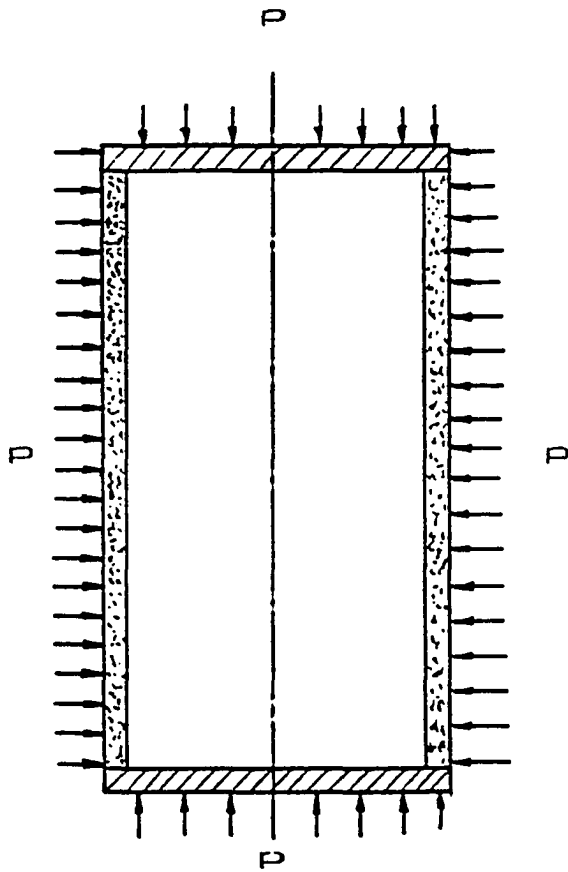


Figure 4 . Schematic diagram of the external pressure test.

3. THEORETICAL ANALYSIS

The experimental-investigation failure results are compared with the following existing criteria.

Tresca and Coulomb-Mohr Criteria: It is generally assumed that plastic flow or failure occurs when, on any plane at any point in the rock mass, the maximum shear stress τ reaches an amount that depends linearly upon the cohesive stress C , and the normal stress σ on the failure plane, and is given by:

$$\tau = C + \sigma \tan \phi \quad (1)$$

This equation was first suggested by Coulomb in 1773. The angle ϕ is known as the angle of internal friction of rock. If ϕ is zero, then equation (1) represents Tresca's yield criterion. The constants C and ϕ can be looked upon simply as parameters which characterize the total resistance of the rock medium to shear. In order to express (1) in terms of principal stress components σ_1 , σ_2 and σ_3 , appropriate for general treatment of three-dimensional problems, one uses the graphical representation of stress due to Mohr. In the Mohr diagram (Fig. 5) the normal stress σ and the shearing stress τ are used as coordinates.

The values of σ , τ satisfying the Coulomb yield criterion (1) are represented in Fig. 5 by two straight lines OE and EF, the latter inclined at angle ϕ to the positive σ axis. If a state of stress σ_1 , σ_2 , σ_3 is such that the Mohr circles lie within the wedge-shaped region (OEF), the rock remains in the linear elastic range. Plastic flow or fracture of rocks occurs for any stress state at or outside this boundary. In terms of principal stresses, the criterion is given by equation (2)

$$(\sigma_1 - \sigma_3)/2 = \{(\sigma_1 + \sigma_3)/2\} \sin \phi + C \cos \phi \quad (2)$$

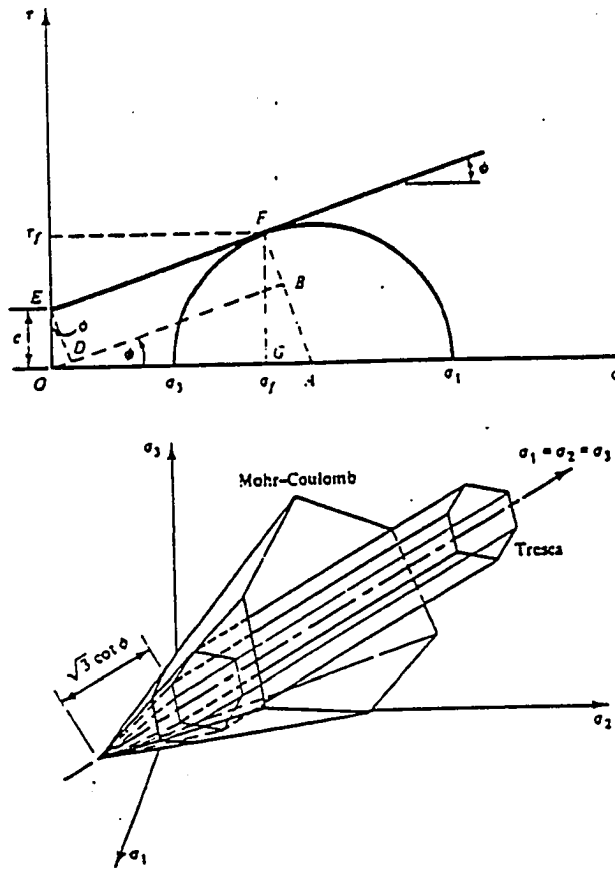


Figure 5 . Coulomb - Mohr Criterion.

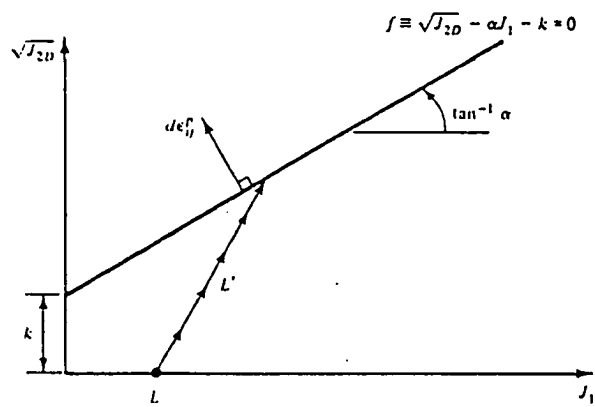


Figure 6 . Drucker and Prager Criterion.

Equation (2) represents a straight line with $(\frac{\sigma_1 - \sigma_3}{2})$ as the ordinate and $(\frac{\sigma_1 + \sigma_3}{2})$ as the abscissa.

Von Mises and Drucker-Prager: The Von Mises criterion may be written in terms of the second invariant of the deviatoric stress tensor J_{2d} and the principal stresses σ_1 , σ_2 , and σ_3 . It is expressed by the equation:

$$J_{2d} = \frac{1}{6} [(\sigma_1 - \sigma_2)^2 + (\sigma_2 - \sigma_3)^2 + (\sigma_3 - \sigma_1)^2] = K^2 \quad (3)$$

where K is the yield stress in pure shear. A modification of the above equation for rocks was proposed by Drucker and Prager (11) in 1952. This is given by equation (4), and is graphically represented in Figure 6.

$$\sqrt{J_{2d}} - \alpha J_1 - K = 0 \quad (4)$$

where J_1 is the first invariant of the stress tensor and α and K are material parameters. In order to establish the failure envelope for a material it is necessary to perform laboratory tests up to failure conditions.

Relationship Between Young's Modulus, Poisson's Ratio, and Shear Modulus for a Bimodular Rock: A bimodular rock is defined as one which has different Young's modulus in tension and compression. Hence, the normal equation relating Young's modulus, Poisson's ratio, and shear modulus is no longer true for a bimodular rock. Let E_t , ν_t , and E_c , ν_c be the Young's moduli and Poisson's ratios in tension and compression, respectively, and G the shear modulus. Then for a bimodular rock the equation relating these three material constants was first proposed in 1965 by Ambartsumyan (48). In 1968 Bert derived it in a different way, and this equation was verified experimentally using Novak's experimental results (49). This equation can be derived as follows: Figure 7a represents an element in the state of pure shear. Figure

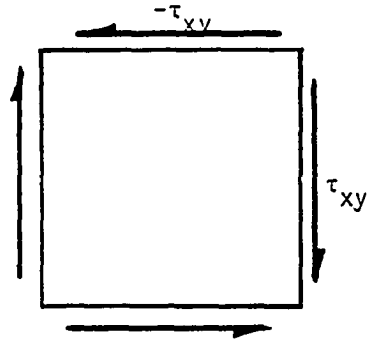


Figure 7 a. Element in state of pure shear.

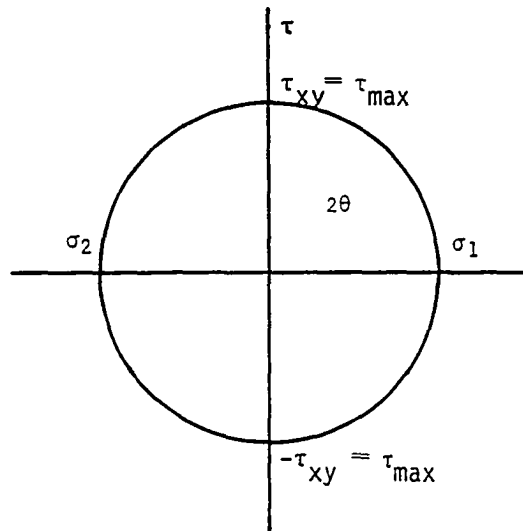


Figure 7 b. Mohr's stress circle for pure shear

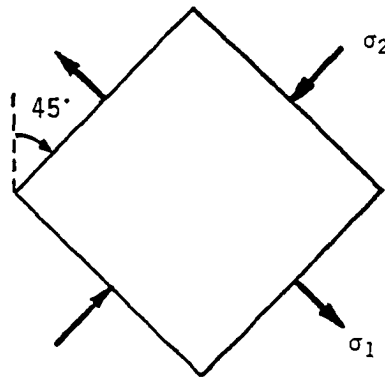


Figure 7 c. Element oriented with its faces parallel to the principal plane.

7b is the Mohr's circle representation for the corresponding state of stress and Figure 7c shows the element oriented with its faces parallel to the principal planes. Here σ_1 and σ_2 are the maximum and the minimum principal stresses respectively. Expressing this biaxial state of stress in terms of Hooke's law one obtains:

$$\epsilon_1 = \frac{\sigma_1}{E_t} - \nu_c \frac{\sigma_2}{E_c} \quad (5)$$

$$\epsilon_2 = \frac{\sigma_2}{E_c} - \nu_t \frac{\sigma_1}{E_t} \quad (6)$$

$$\gamma_{xy} = \frac{\tau_{xy}}{G} \quad (7)$$

Now in case of pure shear $\sigma_1 = +|\tau_{xy}|$ and $\sigma_2 = -|\tau_{xy}|$ equations (5) and (6) can be rewritten as,

$$\epsilon_1 = \tau_{xy} \left(\frac{1}{E_t} + \frac{\nu_c}{E_c} \right) \quad (8)$$

and
$$\epsilon_2 = -\tau_{xy} \left(\frac{1}{E_c} + \frac{\nu_t}{E_t} \right) \quad (9)$$

The maximum shear strain

$$\gamma_{xy} = \epsilon_1 - \epsilon_2 = \frac{\tau_{xy}}{G} \quad (10)$$

Substituting (8) and (9) in (10) one gets

$$\frac{1}{G} = \frac{1}{E_t} (1 + \nu_t) + \frac{1}{E_c} (1 + \nu_c) \quad (11)$$

For the special case when $\nu_c = \nu_t$ and $E_c = E_t$ equation (11) reduces to the isotropic elastic case.

IV. EXPERIMENTAL RESULTS AND DISCUSSION

This experimental study was carried out in two main stages. In stage one approximately forty tests were carried out at ambient temperature on hollow rock specimens up to failure to study fracture behavior under different loading conditions and various loading paths. The different loading paths to which the rock specimen were subjected are tension, torsion, tension followed by torsion, torsion followed by tension, combined tension-torsion, compression followed by torsion, internal pressure, confining pressure followed by tension, tension followed by confining pressure, compression followed by confining pressure, torsion followed by confining pressure, compression followed by confining pressure followed by torsion, and equal internal external pressure and external pressure. In the second stage twenty additional experiments were performed under the loading conditions and loading paths as described above, but at a temperature of 300°F.

All the tests carried out in stage one are tabulated in Table 1 with the corresponding values of the stress components at failure. Principal stresses calculated from these stress components are tabulated in Table 2. Similar test data for the experiments performed in stage two (i.e. at 300°F) are tabulated in Tables 3 and 4. The coordinate system used is shown in Figure 8.

4a. Experimental Results at Ambient Temperature

From the uniaxial tension test the average tensile strength was measured as 1068 psi, and the average values of the Young's modulus and Poisson's ratio were measured to be 6.68×10^6 psi and 0.178. A typical stress-strain curve for a uniaxial tensile test is as shown in Figure 9. A pure torsion test measured the shear modulus and the shear strength to be 3.07×10^6 psi and 960 psi respectively. Figure 10 shows a plot of shear stress versus shear strain for a typical torsion test. The average Young's modulus and Poisson's ratio

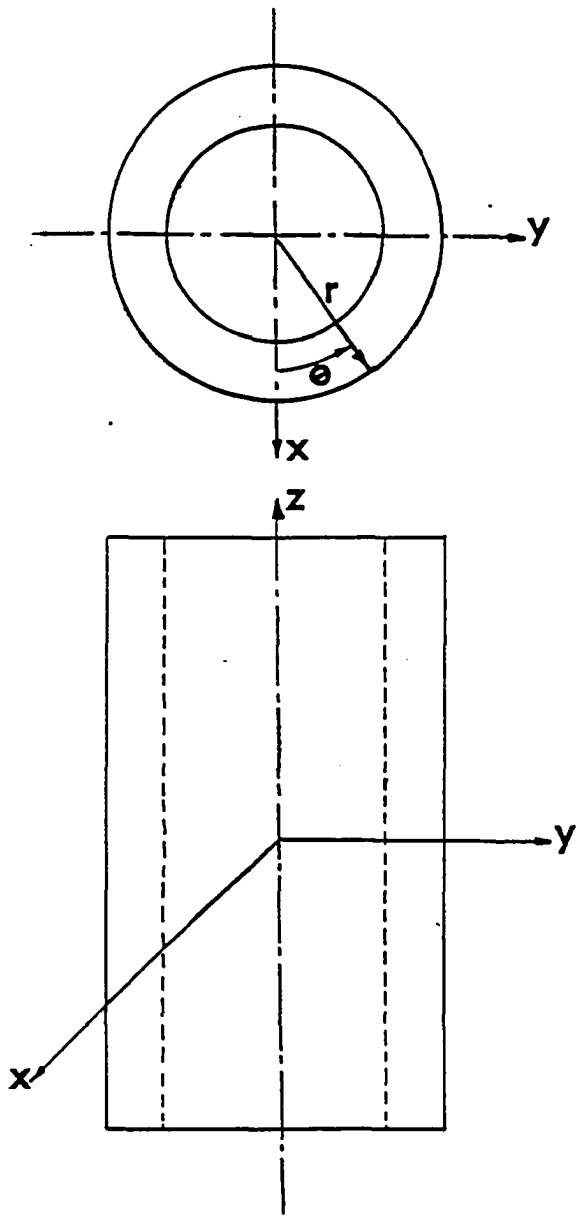


Figure 8 . Coordinate system.

TABLE I

Values of stress components at failure for various tests at ambient temperature.

Experiment number	Experiment type	σ_r psi	σ_θ psi	σ_z psi	$\tau_{z\theta}$ psi
12, 24, 25, 27, 31, 32, 33	Tension	-	-	-1068	-
13, 26, 45, 46	Torsion	-	-	-	960
6	Tension→ Torsion	-	-	-581	405
18	Torsion→ Tension	-	-	-710	525
23	Combined Tension- Torsion	-	-	-599	633
28	Torsion→ Tension	-	-	-1045	216
29	Torsion→ Tension	-	-	-948	327
30	Torsion→ Torsion	-	-	-499	770
34	Torsion→ Tension	-	-	-517	799
35	Torsion→ Torsion→ Tension	-	-	407	814
36	Combined Tension- Torsion	-	-	-1082	117
37	Torsion→ Torsion	-	-	-271	778
42	Compression→ Torsion	-	-	854	1155
43	Compression→ Torsion	-	-	546	1188
44	Compression→ Torsion	-	-	1245	1331
47, 48	External Pressure	+5857	+44119*	+24989	-
49, 50	Internal Pressure	+125*	-841*	+357	-
51	Pressure→ Tension	+1000	+1000	-553	-
52	Pressure→ Tension	+1000	+1000	-880	-
54	Equal Internal- External Pressure	+2500	+2500	-	-
55	Torsion→ Pressure	+1200	+1200	-614	-
56	Compression→ Pressure	+3300	+3300	+1422	-

TABLE I (con't.)

Experiment number	Experiment type	σ_r psi	σ_θ psi	σ_z psi	$\tau_{z\theta}$ psi
57	Torsion→ Pressure	+2800	+2800	-	643
58	Compression→ Pressure	+4500	+4500	+1610	-
59	Compression→ Pressure	+3600	+3600	+1626	-
60	Compression→ Pressure	+6000	+6000	+2779	-
61	Compression→ Pressure→ Torsion	+4300	+4300	+3042	445
62	Compression→ Pressure→ Torsion	+3000	+3000	+3756	884
63	Equal Inter- nal-External Pressure	+2800	+2800	-	-
64	Torsion→ Pressure	+1400	+1400	-	472
65	Pressure→ Torsion	+2000	+2000	-	425
66	Compression→ Pressure	+5000	+5000	+2805	-
67	Compression→ Pressure→ Torsion	+5000	+5000	+2300	1429
68	Compression→ Pressure	+3500	+3500	+1457	-
69	Compression→ Pressure	+6000	+6000	+3475	-
70	External Pressure	+6129*	45051*	+25590*	-
71	Equal Inter- nal-External Pressure	+2600	+2600	-	-

Note: $\tau_{r\theta} = \tau_{rz} = 0$ for all tests. Sign Convention: compression: positive; tension: negative.

* Average value

TABLE II

Principal stresses at failure for various tests at ambient temperature.

Experiment number	Experiment type	σ_3 psi	σ_2 psi	σ_1 psi	J_1 psi	$\sqrt{J_{2d}}$ psi	U_0 psi
12, 24, 25, 27, 31, 32, 33	Tension	-1068	-	-	-1068	617	0.08
13, 26, 45, 46	Torsion	- 960	0	+960	0	960	0.15
6	Tension→ Torsion	- 789	0	+208	-581	526	0.052
18	Tension→ Tension	- 988	0	+289	-699	670	0.0826
23	Combined Tension- Torsion	-1027	0	+428	-599	748	0.0985
28	Tension→ Tension	-1088	0	+43	-1045	641	0.089
29	Tension→ Tension	-1050	0	+102	-948	638	0.085
30	Tension→ Torsion	-1059	0	+560	-499	822	0.115
34	Tension→ Torsion	-1079	0	+562	-517	834	0.119
35	Tension→ Torsion	-1042	0	+635	-407	846	0.12
36	Combined Tension- Torsion	-1109	0	+28	-1081	648	0.093
37	Tension→ Torsion	- 925	0	+654	-271	793	0.104
42	Compression→ Torsion	- 804	0	+1658	+854	1255	0.259
43	Compression→ Torsion	- 946	0	+1492	+546	1229	0.247
44	Compression→ Torsion	- 847	0	+2092	+1245	1513	0.378
47, 48	External Pressure	+5857	+24989	+44119	+74964	19131	117.1
49, 50	Internal Pressure→	- 841	- 358	+125	-1074	483	0.055
51	Pressure→ Tension	- 553	+1000	+1000	+1447	896	0.150
52	Pressure→ Tension	- 880	+1000	+1000	+1120	1086	0.20
54	Equal Inter- nal-External Pressure	0	+2500	+2500	+5000	1443	0.586
55	Pressure→ Pressure	- 614	+1200	+1200	+1786	1047	0.21
56	Compression→ Pressure	1422	3300	3300	8022	1084	0.933

TABLE II (con't.)

Experiment number	Experiment type	σ_3 psi	σ_2 psi	σ_1 psi	J_1 psi	$\sqrt{J_2d}$ psi	U_0 psi
57	Torsion→ Pressure	-162	+2800	+2962	-5600	1740	0.804
58	Compression→ Pressure	+1610	+4500	+4500	-10610	1668	1.732
59	Compression→ Pressure	1629	+3600	+3600	-8826	1140	1.112
60	Compression→ Pressure	+2779	+6000	+6000	-14779	1800	3.09
61	Compression→ Pressure→ Torsion	+2901	+4300	+4442	-11643	1119	1.827
62	Compression→ Pressure→ Torsion	+2412	+3000	+4344	-9756	990	1.4
63	Equal Internal-External Pressure	0	+2800	+2800	-5600	1611	0.736
64	Torsion→ Pressure	-145	+1400	1545	-2800	936	0.22
65	Pressure→ Torsion	-87	+2000	+2087	-4000	1231	0.401
66	Compression→ Pressure	+2805	+5000	+5000	-12805	1267	2.185
68	Compression→ Pressure	+1457	+3500	+3500	-8457	1180	1.046
69	Compression→ Pressure	+3475	+6000	+6000	-15375	1458	3.16
70	External Pressure	+6129	+25590	+45051	-76770	19461	121.87
71	Equal Internal-External Pressure	0	+2600	+2600	-5200	1501	0.631

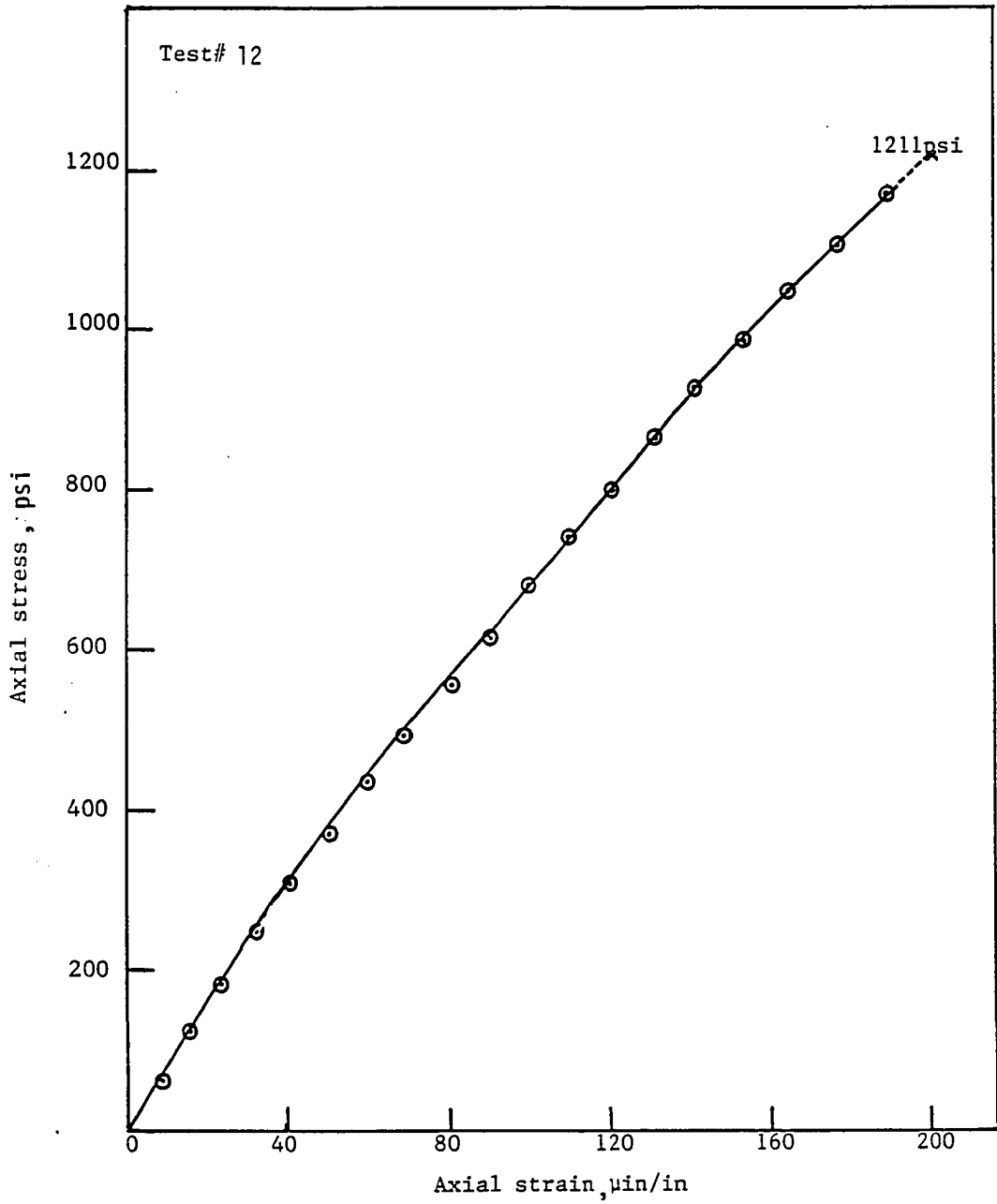


Figure 9 . Uniaxial tensile stress-strain curve for granite at ambient temperature.

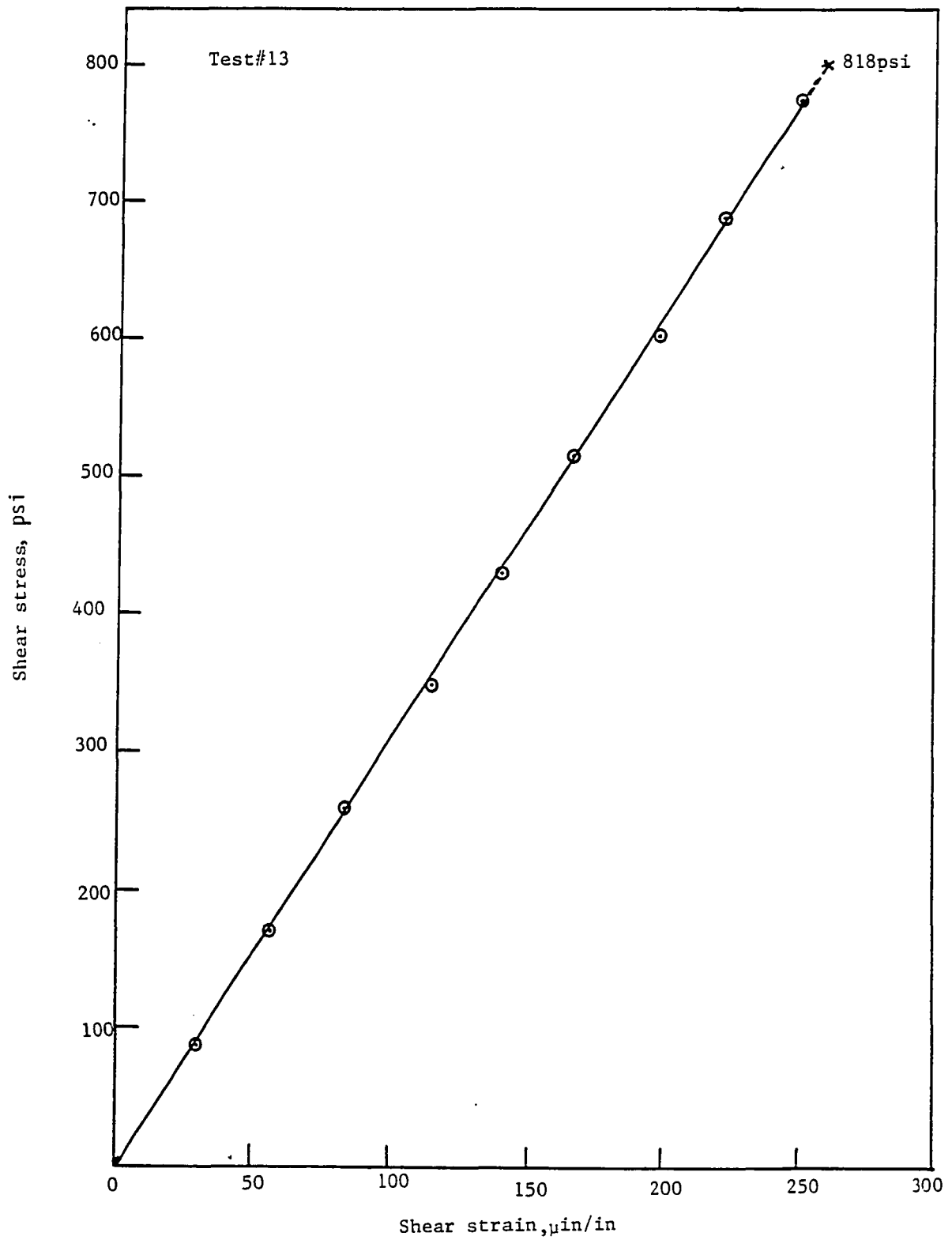


Figure 10. Shear stress-shear strain curve for granite at ambient temperature.

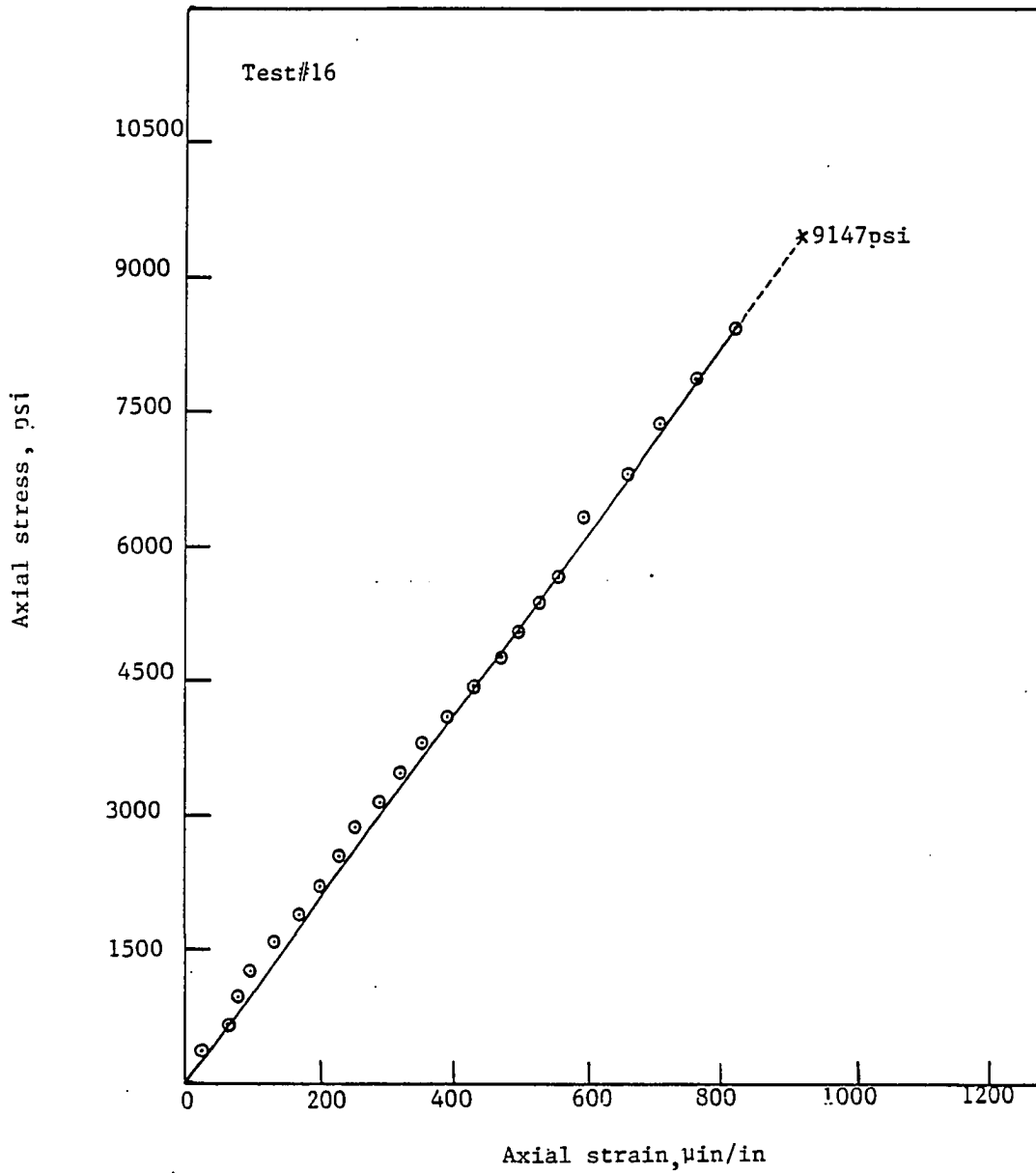


Figure 11. Uniaxial compressive stress-strain curve for granite at ambient temperature.

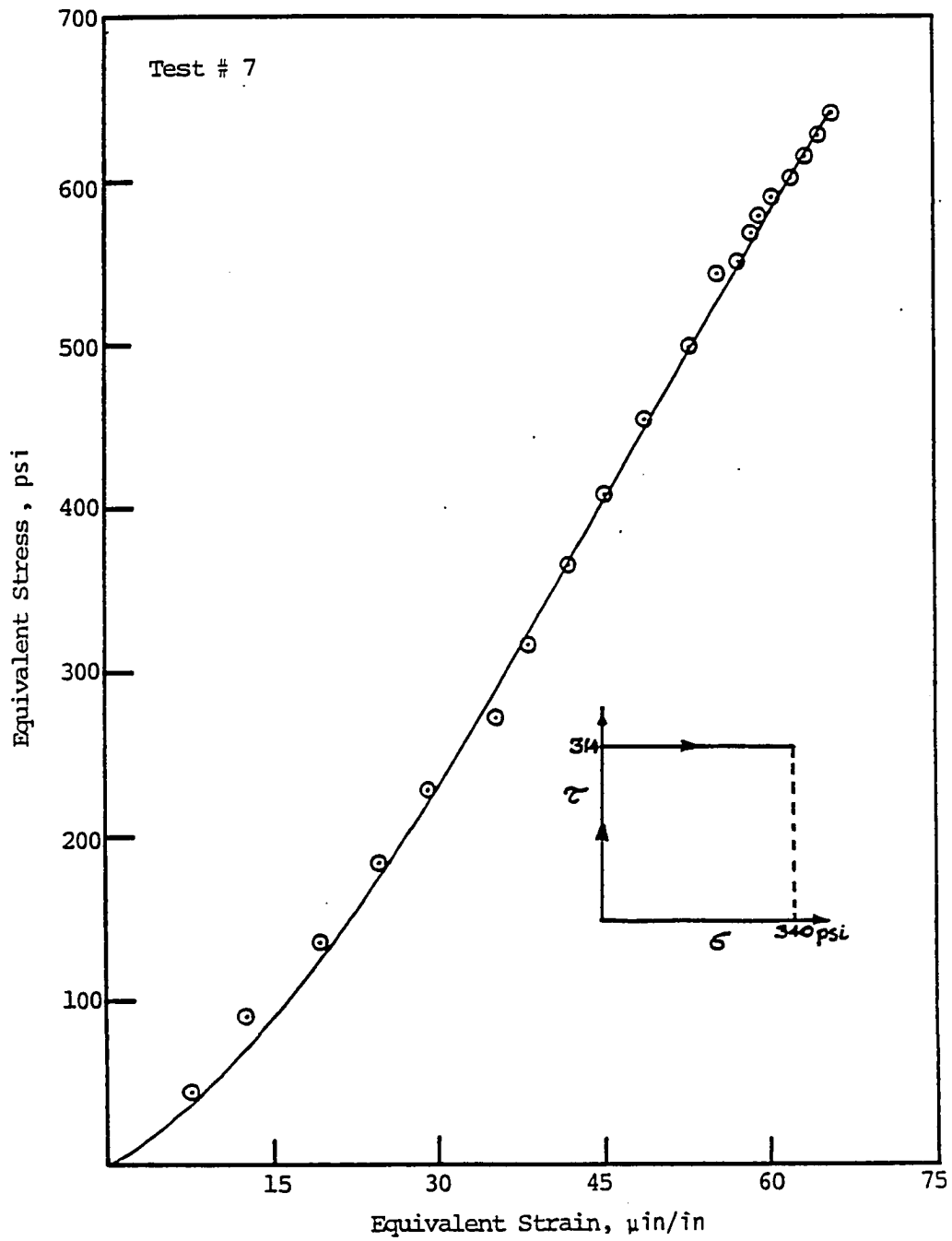


Fig. 12. Quasi-static equivalent stress vs equivalent strain curve.

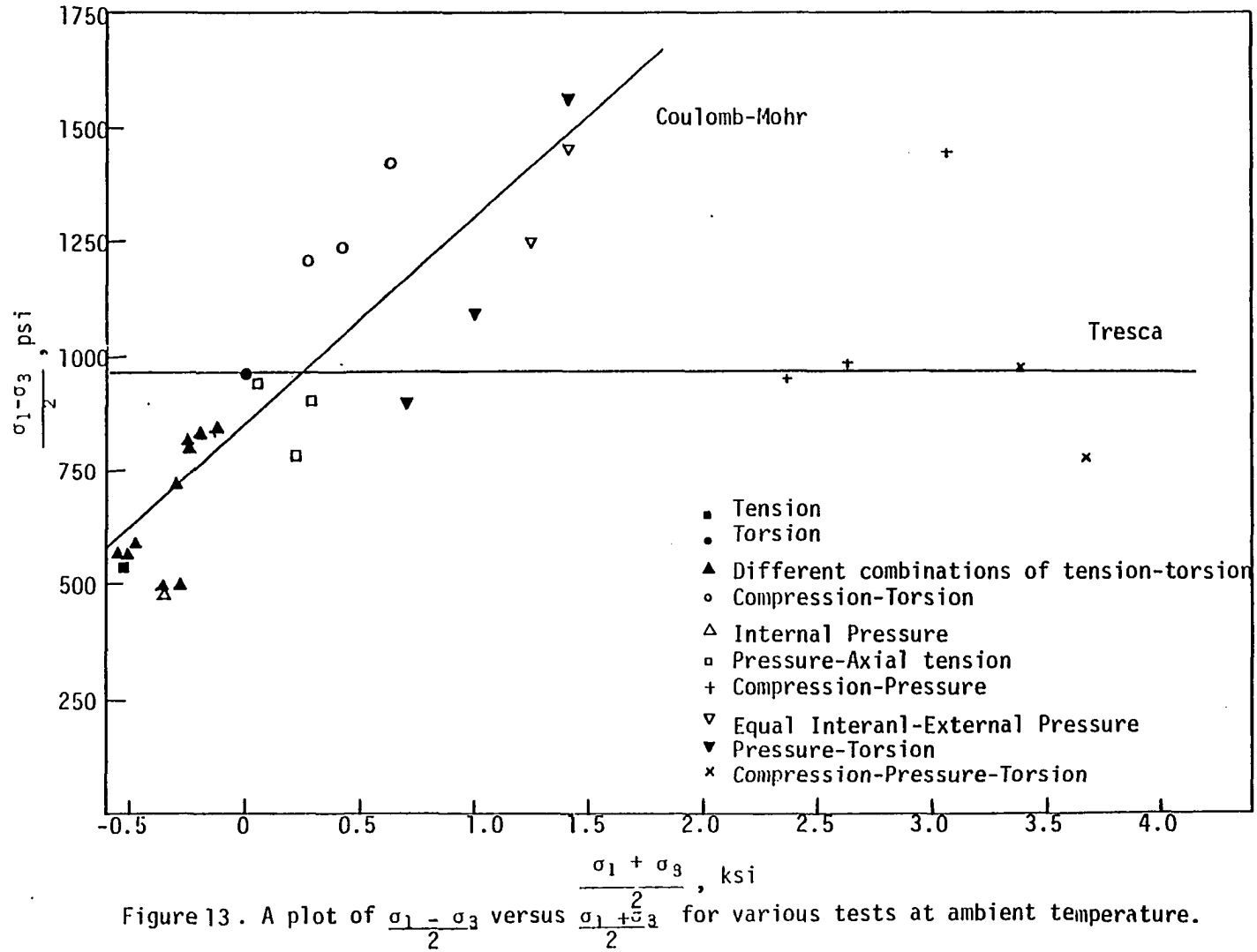
in compression were measured to be 8.63×10^6 psi and 0.196 psi respectively. A typical axial stress-strain curve in uniaxial compression is as shown in Figure 11. The plot of equivalent stress versus equivalent strain for a tension-torsion test is shown in Figure 12.

All the experiments up to test number 44 were carried out under one dimensional or various combinations of two dimensional loading conditions until failure. Beyond test number 44, confining pressure of different magnitudes is introduced with various axial and/or torsional load combinations to produce three dimensional conditions except for test numbers 54, 63, 71 where only an equal internal and external pressure loading condition exists.

The material parameters associated with the failure criteria described in the previous section can now be evaluated. The two parameters associated with the Coulomb-Mohr failure criterion, the angle of internal friction ϕ and the cohesive stress C can be determined using equation (2) and a plot of $\frac{\sigma_1 + \sigma_3}{2}$ versus $\frac{\sigma_1 - \sigma_3}{2}$ [Figure 13]. The parameters associated with the Drucker and Prager failure criterion are evaluated using equation (4) and a plot of J_1 versus $\sqrt{J_{2d}}$ [Figure 14].

The numerical values of these material parameters evaluated from Figures 13 and 14 are as follows:

$$\text{Tresca: } \left(\frac{\sigma_1 - \sigma_3}{2} \right)_{\text{average}} = K = 6.45 \text{ MPa (936 psi)}$$



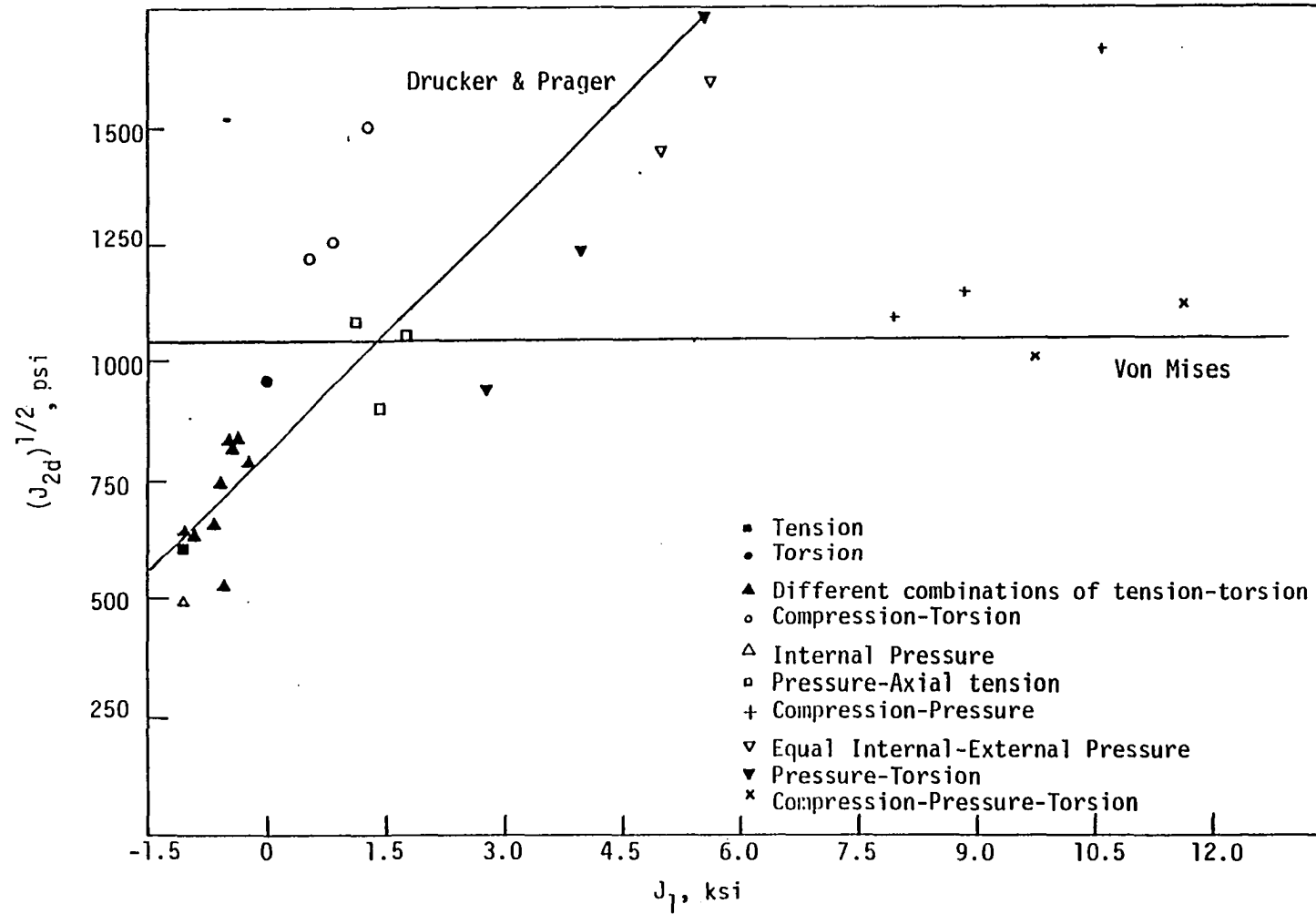


Figure 14 . A plot of $(J_{2d})^{1/2}$ versus J_1 for various tests at ambient temperature.

Coulomb-Mohr: $\phi = 24.14^\circ$

$C = 6.43 \text{ MPa (932 psi)}$

Von Mises: $(\sqrt{J_{2d}})_{\text{average}} = 7.14 \text{ MPa (1035 psi)}$

Drucker and Prager: $K = 5.69 \text{ MPa (825 psi)}$

$\alpha = 0.166$

The plots of $\frac{\sigma_1 + \sigma_3}{2}$ versus $\frac{\sigma_1 - \sigma_3}{2}$ and J_1 versus $\sqrt{J_{2d}}$, as shown in Figures 13 and 14 respectively, reveal that neither of the above mentioned failure criteria is able to predict the experimental failure results over the entire range of stress values at failure. It can be seen further from the plot in Figure 13 that the Coulomb-Mohr criterion agrees well with the experimental data up to a certain value of $\frac{\sigma_1 + \sigma_3}{2}$ but at higher values of $\frac{\sigma_1 + \sigma_3}{2}$ Tresca's criterion seems to dominate the prediction of the failure behavior. An almost similar trend is also observed from the plot in Figure 14. At lower values of J_1 , the Drucker and Prager criterion is able to predict the failure envelope but at higher values of J_1 the experimental data agree much better with the von Mises criterion. Due to these reasons, an attempt was made to develop a failure criterion which will be able to predict the failure behavior over the entire range of stress values. Also this new failure criterion should have the provisions to incorporate bimodular material behavior which is not accounted for in the failure theories discussed in the previous section.

One obvious choice for such a failure criterion is in terms of strain energy density, which can be evaluated from the equation:

$$U_0 = \frac{1}{2E} (\sigma_x^2 + \sigma_y^2 + \sigma_z^2) - \frac{\nu}{E} (\sigma_x \sigma_y + \sigma_y \sigma_z + \sigma_z \sigma_x) + \frac{1}{2G} (\tau_{xy}^2 + \tau_{xz}^2 + \tau_{yz}^2) \quad (12)$$

For bimodular material behavior equation (13), which is the modified version of equation (12), is used to take into consideration the proper value of the material constants in tension and compression.

$$U_0 = \left(\frac{\sigma_x^2}{2E} + \frac{\sigma_y^2}{2E} + \frac{\sigma_z^2}{2E} \right) - \frac{1}{2} [\sigma_x \sigma_y \left\{ \left(\frac{\nu}{E} \right)_{\sigma_x} + \left(\frac{\nu}{E} \right)_{\sigma_y} \right\} + \sigma_y \sigma_z \left\{ \left(\frac{\nu}{E} \right)_{\sigma_y} + \left(\frac{\nu}{E} \right)_{\sigma_z} \right\} + \sigma_z \sigma_x \left\{ \left(\frac{\nu}{E} \right)_{\sigma_z} + \left(\frac{\nu}{E} \right)_{\sigma_x} \right\}] + \frac{1}{2G} (\tau_{xy}^2 + \tau_{yz}^2 + \tau_{zx}^2) \quad (13)$$

This strain energy density is evaluated for the various tests performed and is listed in Table 2. In Figure 15 the experimental values are plotted with J_1 as the abscissa and U_0 as the ordinate for all tests except the external pressure tests (numbers 47, 48, 70). In all tests plotted, the value of J_1 ranged between -1,200 psi to 16,000 psi. It is observed from this plot that a nonlinear relationship exists between U_0 and J_1 . In order to determine this nonlinear relationship between U_0 and J_1 , a least square fit procedure is utilized to determine the equation of the best fit curve. It was determined that the experimental results are best predicted by a cubic equation given by:

$$U_0 = \alpha + \theta J_1 + \tau J_1^2 + \beta J_1^3 \quad (14)$$

where α , θ , τ and β are material parameters and their numerical values for granite tested, are determined to be:

$$\alpha = 0.12097 \text{ psi}$$

$$\theta = 3.087 \times 10^{-5}$$

$$\tau = 8.6 \times 10^{-9} \text{ psi}^{-1}$$

$$\beta = 1.3996 \times 10^{-13} \text{ psi}^{-2}$$

In order to verify the validity and effectiveness of equation (14) to predict failure behavior for values of J_1 above 110 MPa (16,000 psi.), equation (14) is plotted and compared with the experimental results at a very high value of J_1 . This test was on hollow rock core with closed ends and

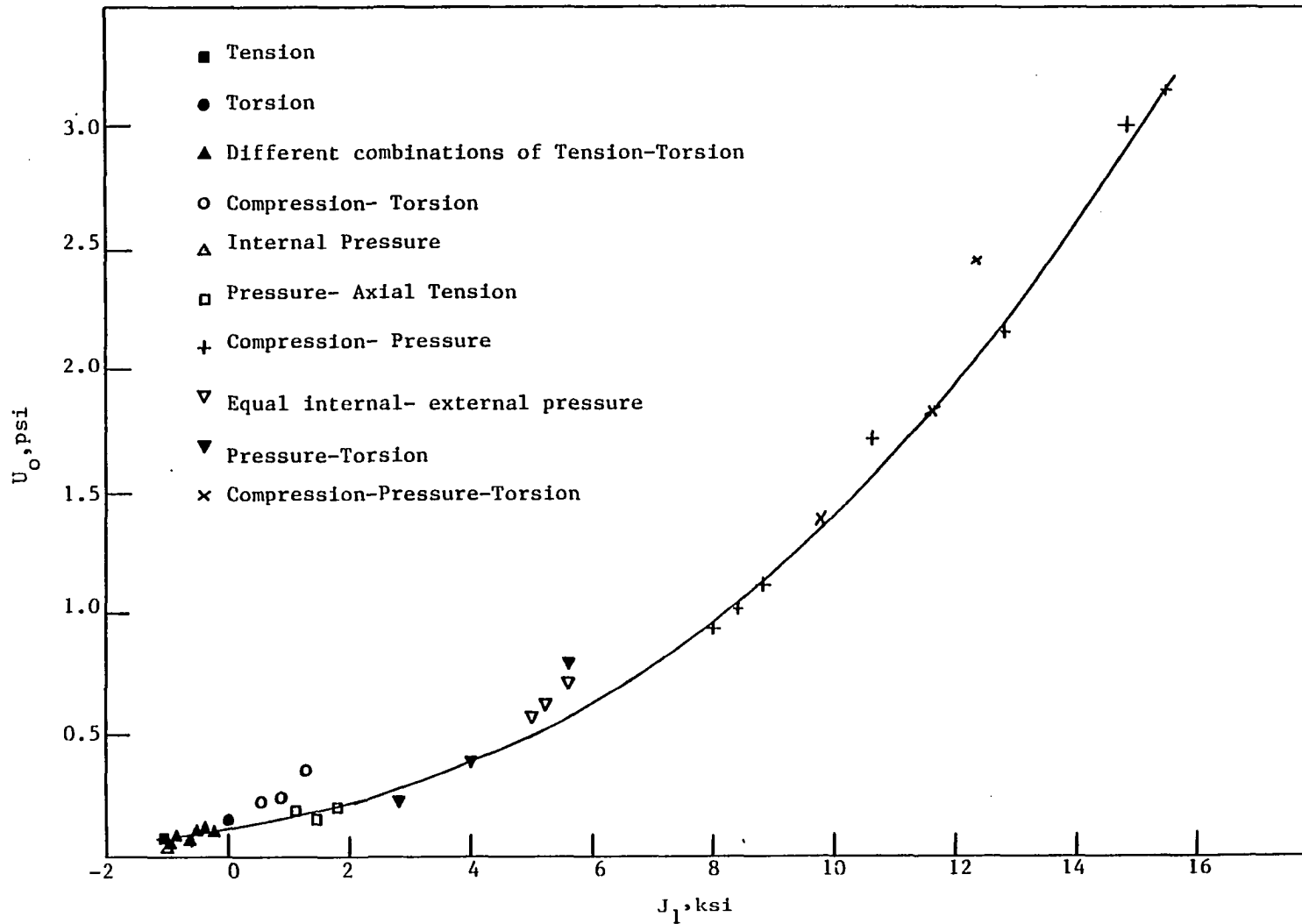


Figure 15. A plot of U_0 versus J_1 .

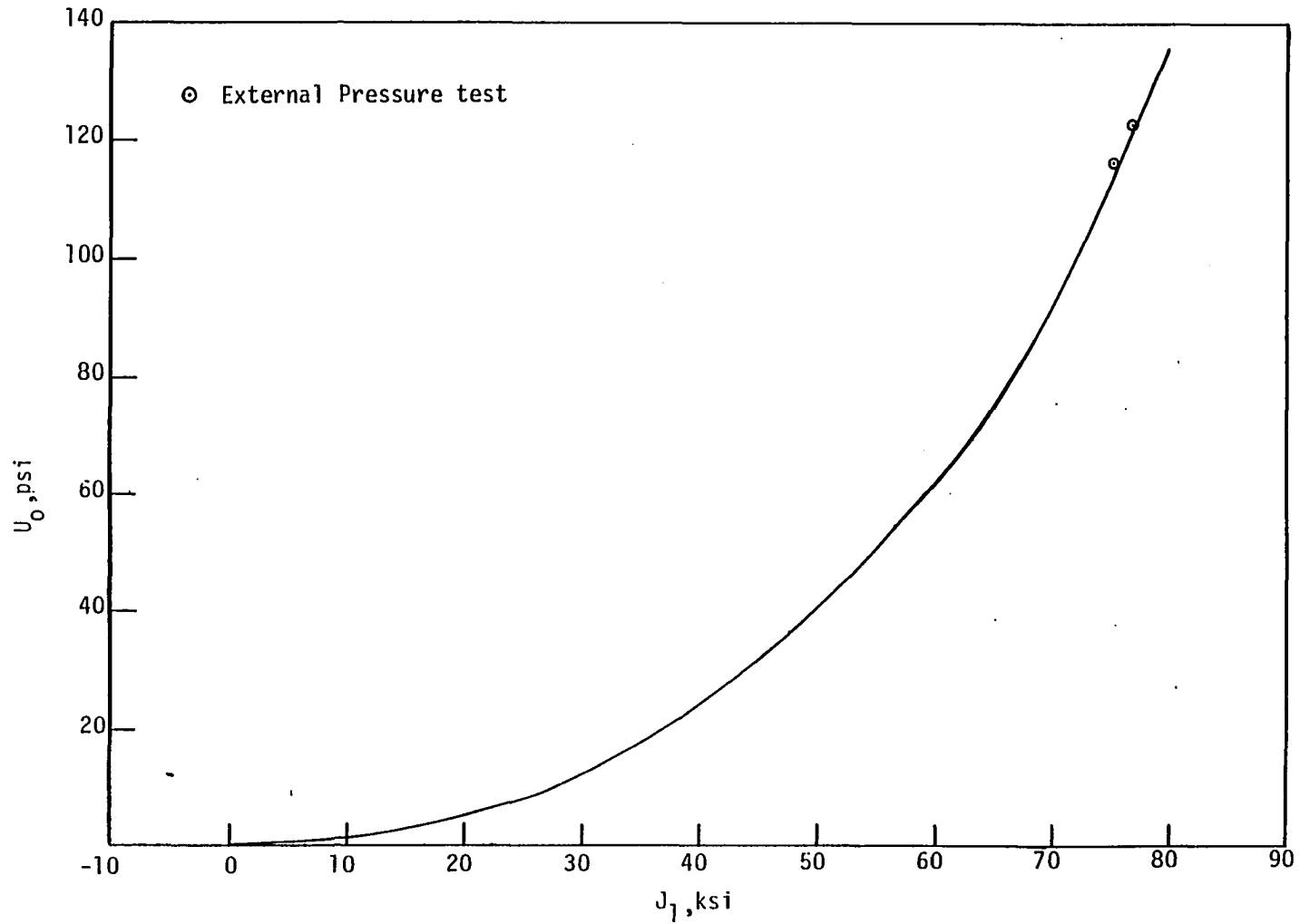


Figure 16. A plot of U_0 versus J_1 showing the external pressure test results at ambient temperature along with a plot of equation (14).

subjected to an external pressure. In this case J_1 has a value of 75,000 psi at failure. A plot of equation (14) and the experimental values of U_0 and J_1 obtained from the external pressure test is shown in Figure 16. This plot confirms the effectiveness of the proposed failure criterion even at high values of J_1 .

4b. Experimental Results at 300° F

Twenty-two experiments were carried out at this temperature and the material properties of the rock were determined and the stress components at failure were measured. From the uniaxial tension test the average tensile strength was measured at 706 psi, and the average values of the Young's modulus and Poisson's ratio were measured to be 4.47×10^6 psi and 0.228. A typical stress-strain curve for a uniaxial tension test is as shown in Figure 17. In a pure torsion test the shear modulus and the shear strength were determined to be 3.035×10^6 psi and 778 psi respectively. Figure 18 shows a plot of shear stress versus shear strain for a typical torsion test at 300° F. Young's modulus and Poisson's ratio in compression at this temperature were measured to be 7.03×10^6 psi and 0.251 respectively. Figure 19 shows a plot of a typical axial stress-strain curve in compression.

Experiments number 74 to 84 were performed either under one dimensional or two dimensional loading conditions. Test numbers 85-97 represent three dimensional loading experiments at 300° F. In these experiments, confining pressure of different magnitudes is introduced with various axial and/or torsional load combinations to produce three dimensional loading conditions. The values of the stress components at failure for these tests are tabulated in Table 3. Corresponding values of the principal stresses are then calculated along with total strain energy density and are tabulated in Table 4. Now in order to compare the experimental results at 300° F with the

TABLE III

Values of stress components at failure for various test at 300° F.

Experiment number	Experiment type	σ_r psi	σ_θ psi	σ_z psi	$\tau_{z\theta}$ psi
74, 76	Torsion	-	-	-	774*
75, 77	Tension	-	-	-706*	-
78	Tension→ Torsion	-	-	-410	666
79	Tension→ Tension	-	-	-547	379
82	Compression→ Torsion-	-	-	+691	1085
83	Compression→ Torsion	-	-	+473	1163
84	Equal Internal External Pressure	+1400	+1400	-	-
85	Compression→ Pressure	+1650	+1650	+1154	-
86	Torsion→ Pressure	+1200	+1200	-	584
87	Compression→ Torsion→	-	-	+671	907
88	Compression→ Torsion→ Pressure	+1350	+1350	+671	560
89	Compression→ Pressure	+2800	+2800	+1562	-
90	Tension→ Pressure	+800	+800	-244	-
91	Compression→ Pressure	+4000	+4000	+2904	-
92	Compression→ Pressure	+4500	+4500	+3401	-
93	External Pressure	+3500*	+29811*	+16441	-
94	Compression→ Pressure	+4000	+4000	+2885	-
95	External Pressure	3671*	32444*	18133	-
96	External Pressure	3878*	32872	18375	-
97	Compression→ Pressure	5200	5200	4297	-

Note: $\tau_{r\theta}$, = τ_{rz} = 0 for all test; Sign Convention: compression: positive; tension: negative.

* Average values

TABLE IV

Principal stresses at failure for various tests at 300° F.

Experiment number	Experiment type	σ_3 psi	σ_2 psi	σ_1 psi	J_1 psi	$\sqrt{J_{2d}}$ psi	U_0 psi
74, 76	Torsion	-778	0	+778	0	778	0.0997
75, 77	Tension	-706	-	-	-706	408	0.055
78	Tension→ Torsion	-902	-	+492	-410	707	0.0919
79	Tension→ Torsion	-741	-	-194	+547	493	0.057
82	Compression→ Torsion	-793	0	+1484	+691	1156	0.228
83A	Compression→ Torsion	-950	0	+1423	+473	1194	0.239
84	Equal Internal External Pressure	0	+1400	+1400	+2800	808	0.208
85	Compression→ Pressure	+1154	+1650	+1650	+4454	286	0.248
86	Tension→ Pressure	-237	+1200	+1437	+2400	906	0.209
87	Compression→ Torsion→	-632	-	+1303	+671	987	0.167
88	Compression→ Torsion→ Pressure	+356	+1350	+1666	+3371	684	0.213
89	Compression→ Pressure	+1562	+2800	+2800	+7162	715	0.697
90	Tension→ Pressure	-244	+800	+800	+1356	603	0.089
91	Compression→ Pressure	+2904	4000	4000	+10906	633	1.48
92	Compression→ Pressure	+3401	+4500	+4500	+12401	636	1.89
93	External Pressure	+3500	+16441	+29811	+49752	13156	57.9
94	Compression→ Pressure	+2885	+4000	+4000	+10885	644	1.462
95	External Pressure	3671	18133	32444	54248	14387	71.36
96	External Pressure	3878	18375	32872	55125	14497	73
97	Compression→ Pressure	4297	5200	5200	14697	521	2.58

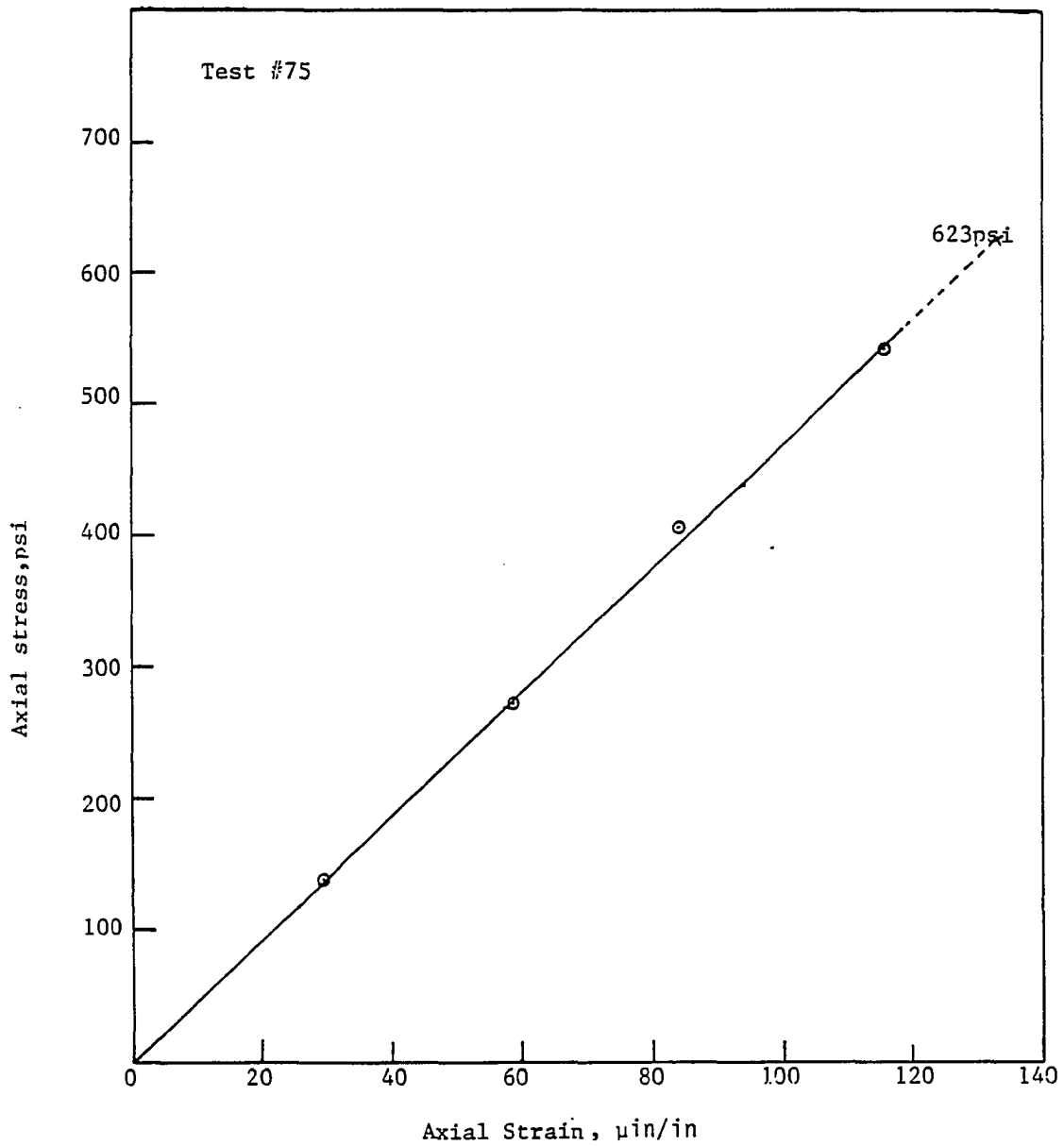


Figure 17. Uniaxial tensile stress-strain curve for granite at 300°F.

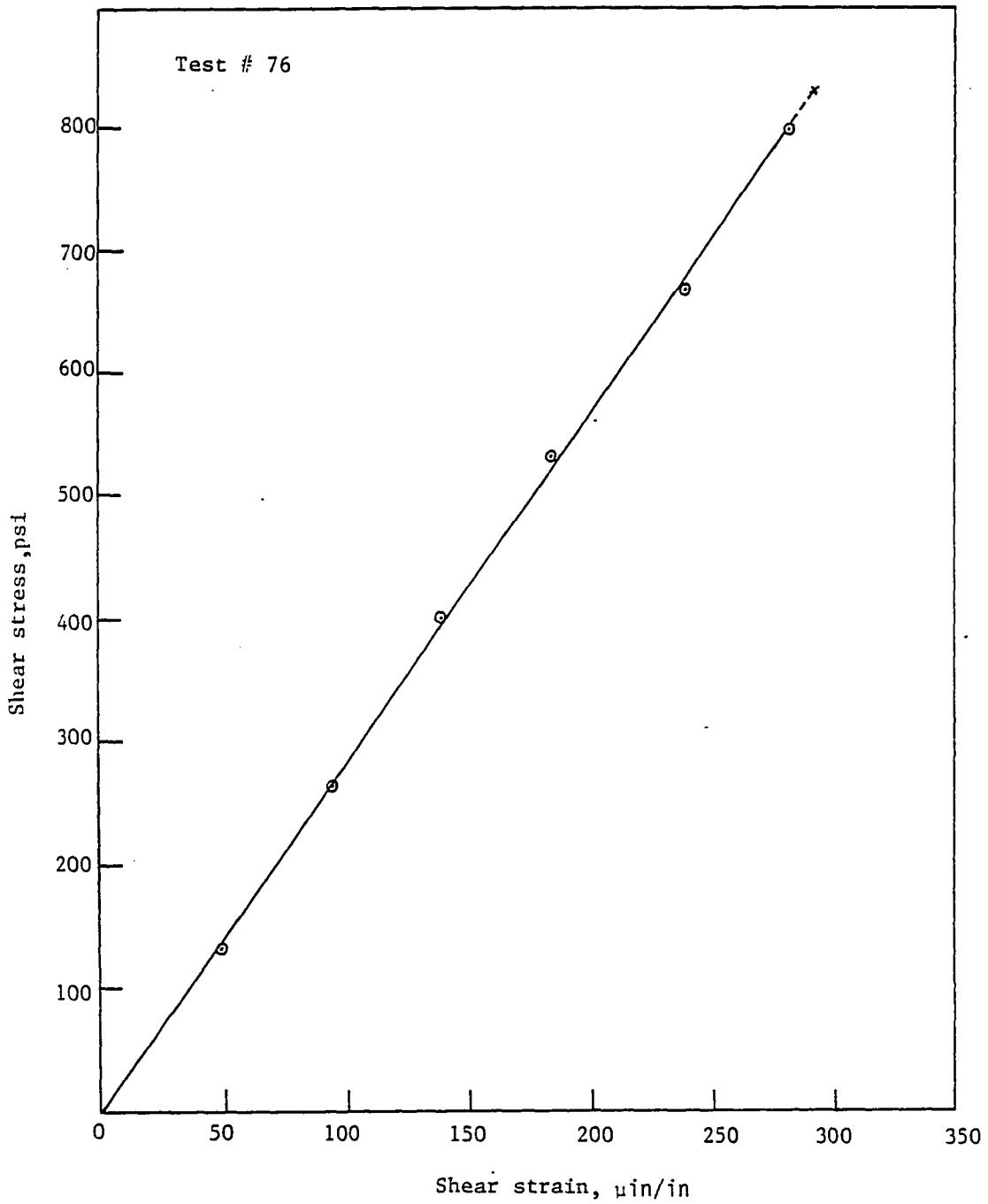


Figure 18. Shear stress-shear strain plot for granite at 300°F

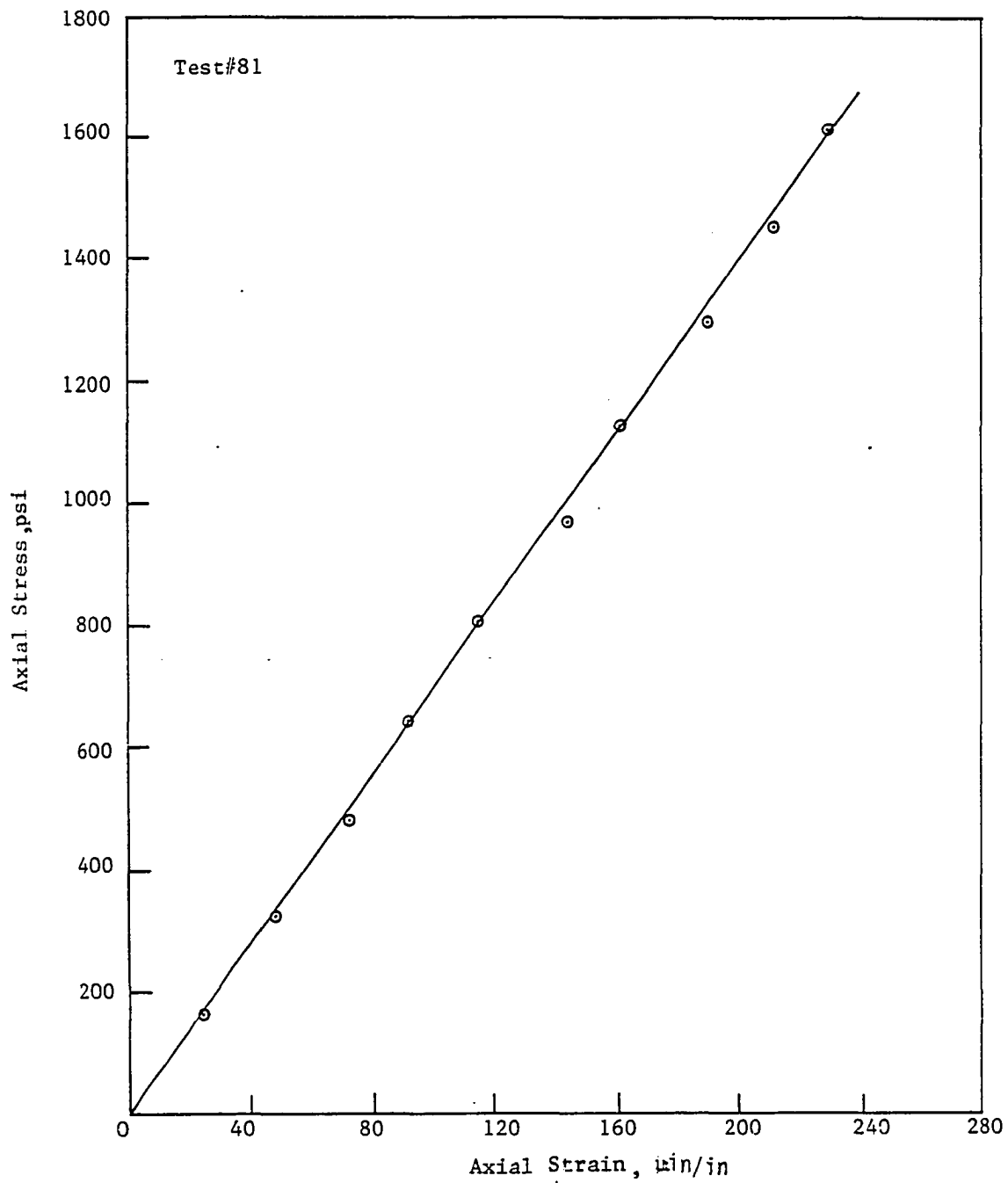


Figure 19. Uniaxial compressive stress-strain curve for granite at 300°F.

failure criteria described in chapter 3, $\frac{\sigma_1 + \sigma_3}{2}$ versus $\frac{\sigma_1 - \sigma_3}{2}$ and J_1 versus $\sqrt{J_2}$ are plotted in Figures 20 and 21 respectively. The plots in Figures 20 and 21 when compared with the failure criteria of Coulomb-Mohr and Drucker and Prager respectively reveal that neither of the two are able to predict the failure of rock over the entire range of stresses at 300° F. Now comparing the plots in Figures 20 and 21 with the plots in Figures 13 and 14 respectively one can observe that at high temperature also the Coulomb-Mohr criterion agrees well with the experimental data for lower values of $\frac{\sigma_1 + \sigma_3}{2}$, but at higher values of $\frac{\sigma_1 + \sigma_3}{2}$ the experimental results are in better agreement with Tresca's criterion. A similar trend is observed when the plot in Figures 21 is compared with the Drucker and Prager and Von Mises criteria.

Since none of the above failure criteria are able to predict the failure of rock over the entire range of stress values at 300° F., a similar procedure to the one used at ambient temperature is adopted, and the experimental results are plotted with U_0 as the ordinate and J_1 as the abscissa to compare the experimental results with the proposed new failure criterion as given by equation (14). This plot of U_0 versus J_1 is given in Figure 22; a nonlinear relationship between U_0 and J_1 is observed from this plot and a similar procedure of least square fit is adopted to determine the equation of the best-fit curve. A third-order cubic equation as given by equation (14) gave the best fit, and numerical values of the material parameters in this case were evaluated to be

$$\alpha = 0.115 \text{ psi}$$

$$\theta = 1.9 \times 10^{-5}$$

$$\tau = 4.62 \times 10^{-9} \text{ 1/psi}$$

$$\beta = 4.46 \times 10^{-13} \text{ 1/psi}^2$$

In order to verify the validity of equation (14), incorporating the above material parameters to predict failure behavior at 300° F for higher values of

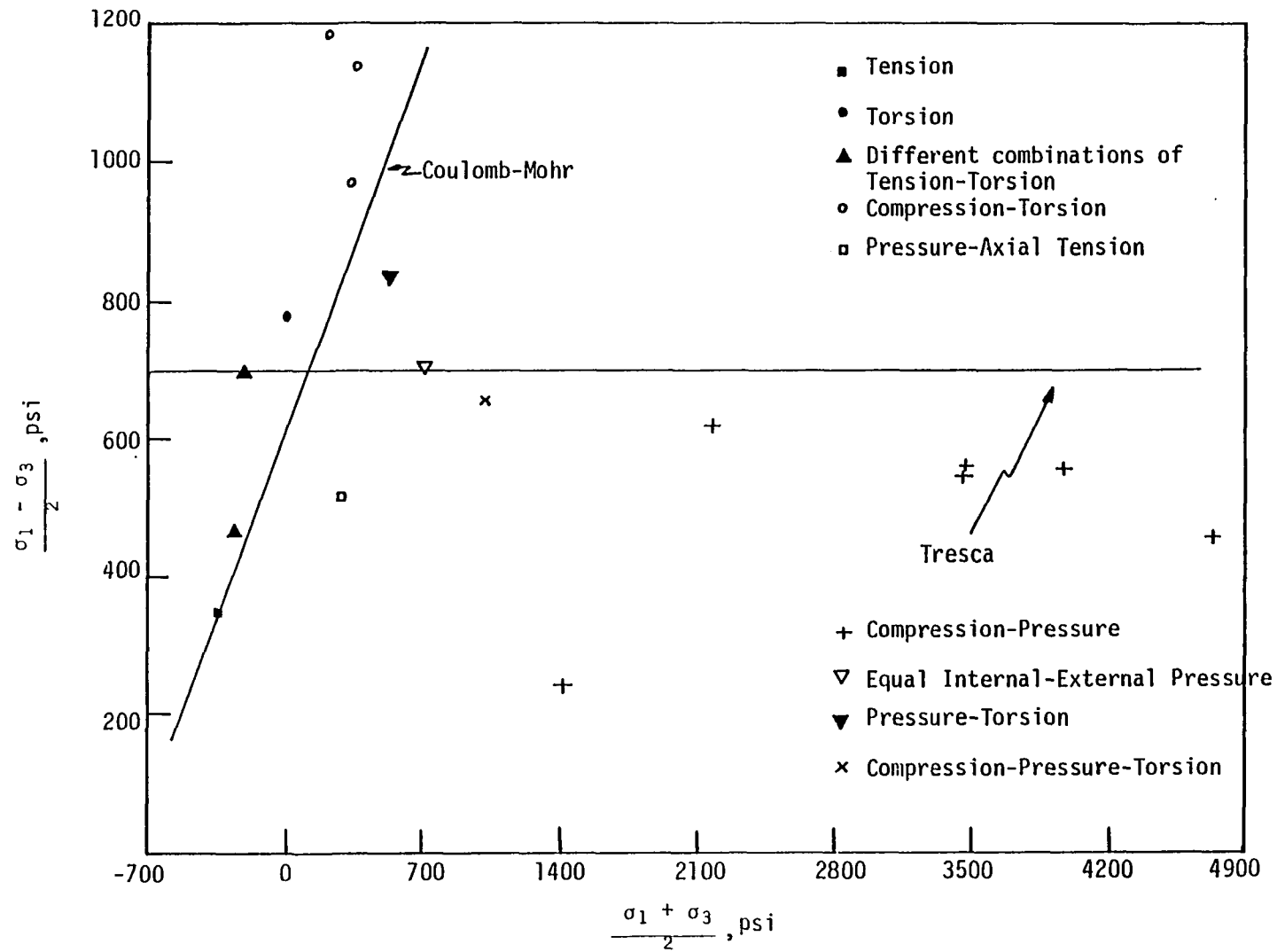


Figure 20. A plot of $\frac{\sigma_1 - \sigma_3}{2}$ versus $\frac{\sigma_1 + \sigma_3}{2}$ for various tests at 300°F.

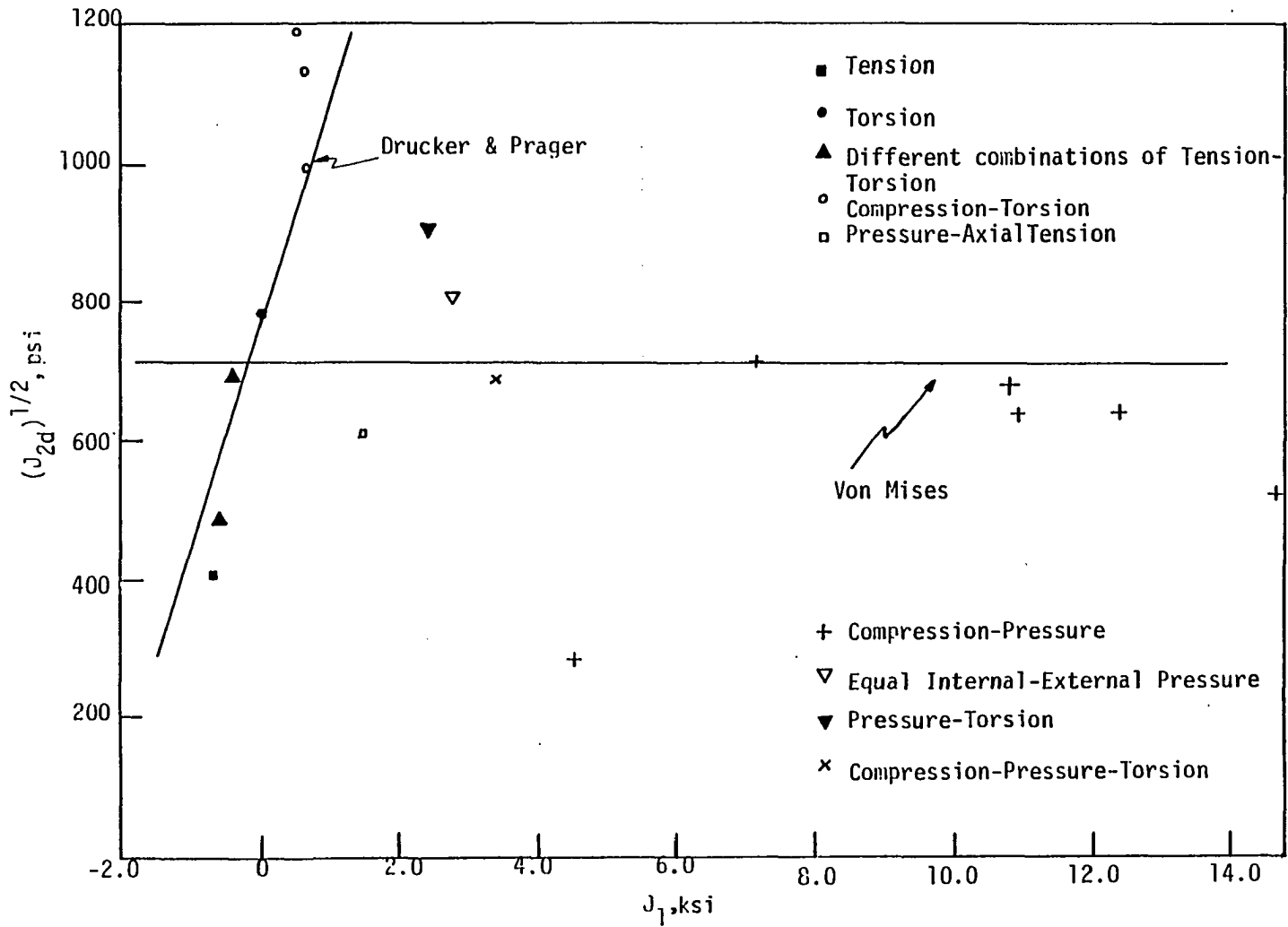


Figure 21. A plot of $(J_{2d})^{1/2}$ versus J_1 for various tests at 300°F.

J_1 equation (14) is plotted and compared with the experimental results of the external pressure tests at 300° F. The plot comparing the values is given in Figure 23, which once again confirms the effectiveness of the proposed failure criterion not only at high values of J_1 but also at high temperature. In order to study the relationships between the constants, α , θ , τ , and β and temperature a combined plot of U_0 versus J_1 is made for all the tests at ambient temperature and at 300° F and is given in Figure 24. The scatter observed in the plot is Figure 24 between the values at ambient temperature and at 300° F was so minimal that we arrived at a preliminary conclusion that the constants α , θ , τ , and β were temperature independent, at least up to 300° F. Least square fit procedure is once again utilized to determine one common equation of the best fit curve for all the results at ambient temperature as well as at 300° F. The constants α , θ , τ , and β for this equation are given as follows.

$$\alpha = 0.1152 \text{ psi}$$

$$\theta = 2.995 \times 10^{-5}$$

$$\tau = 7.8 \times 10^{-9} \text{ 1/psi}$$

$$\beta = 1.9366 \times 10^{-13} \text{ 1/psi}^2$$

The plot of this equation and the experimental results are given in Figure 24. The results of the external pressure test at ambient temperature and at 300° F are plotted along with the above equation in Figure 25. Figures 24 and 25 confirm the effectiveness of the proposed failure criterion to predict the failure behavior of granite under wide range of stresses and at different temperatures.

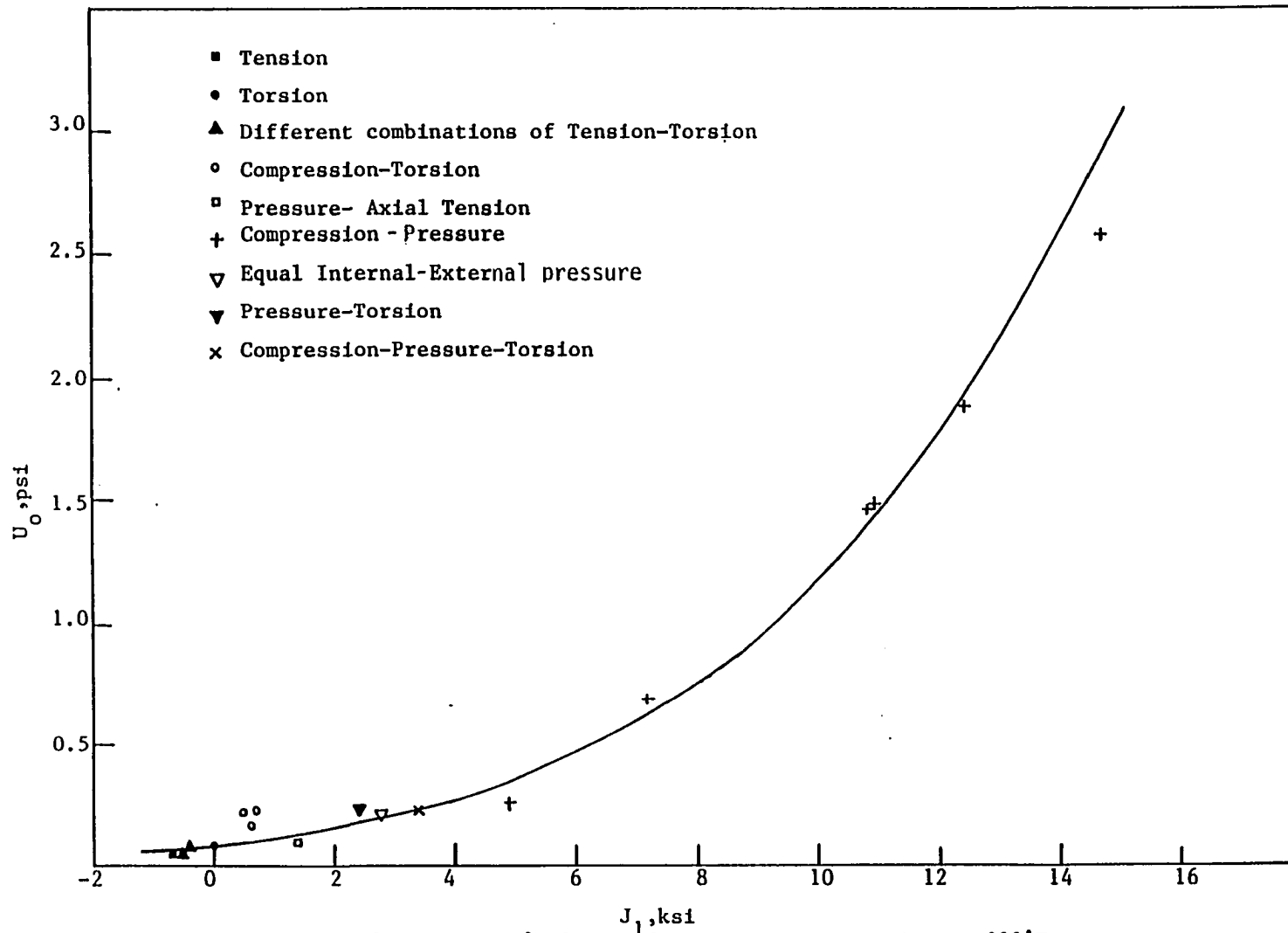


Figure 22. A plot of U_0 versus J_1 for different tests on granite at 300°F.

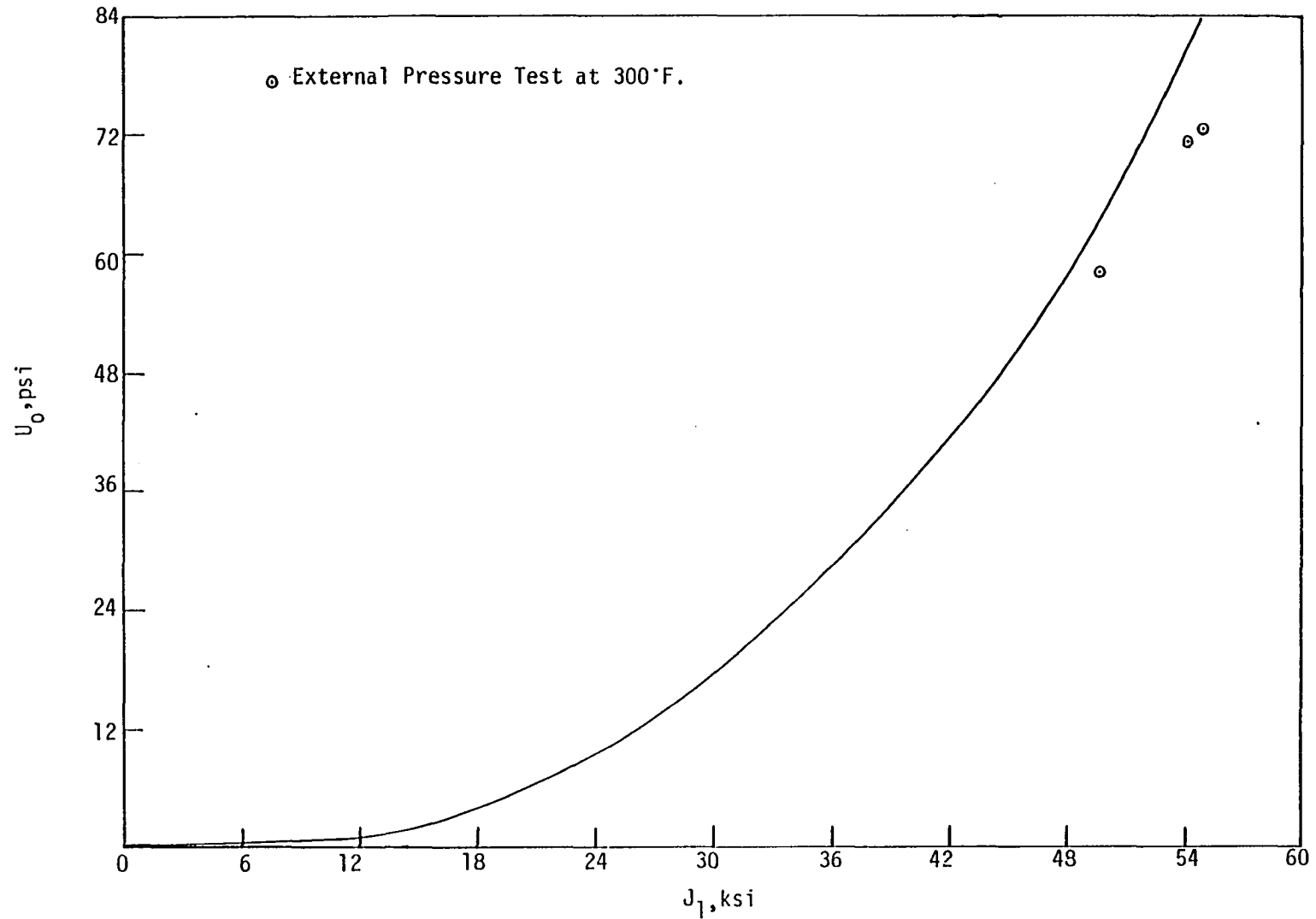


Figure 23. A plot of U_0 versus J_1 for the results of external pressure tests at 300°F.

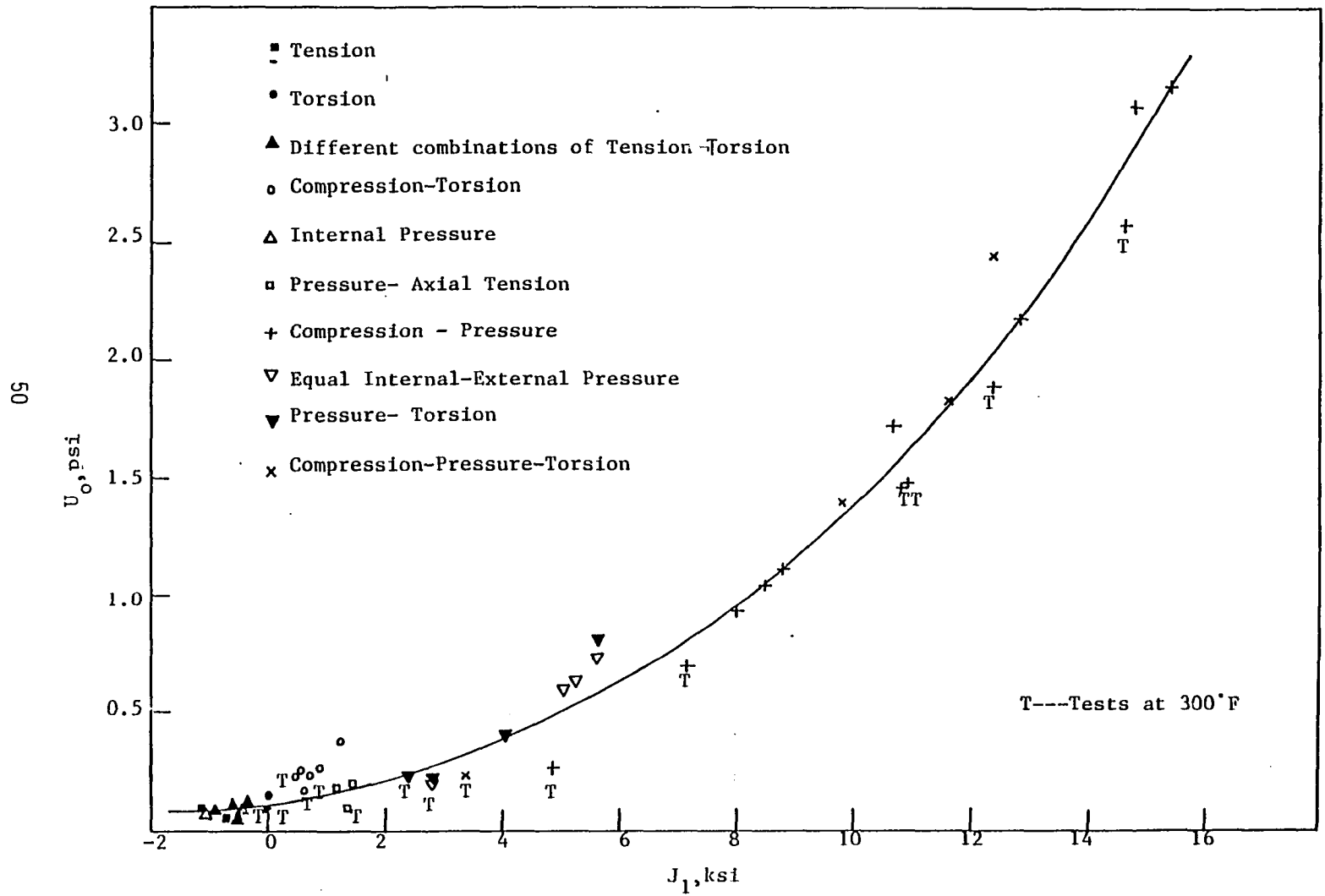


Figure 24. A plot of U_0 versus J_1 for all the tests on granite at ambient temperature and at 300°F.

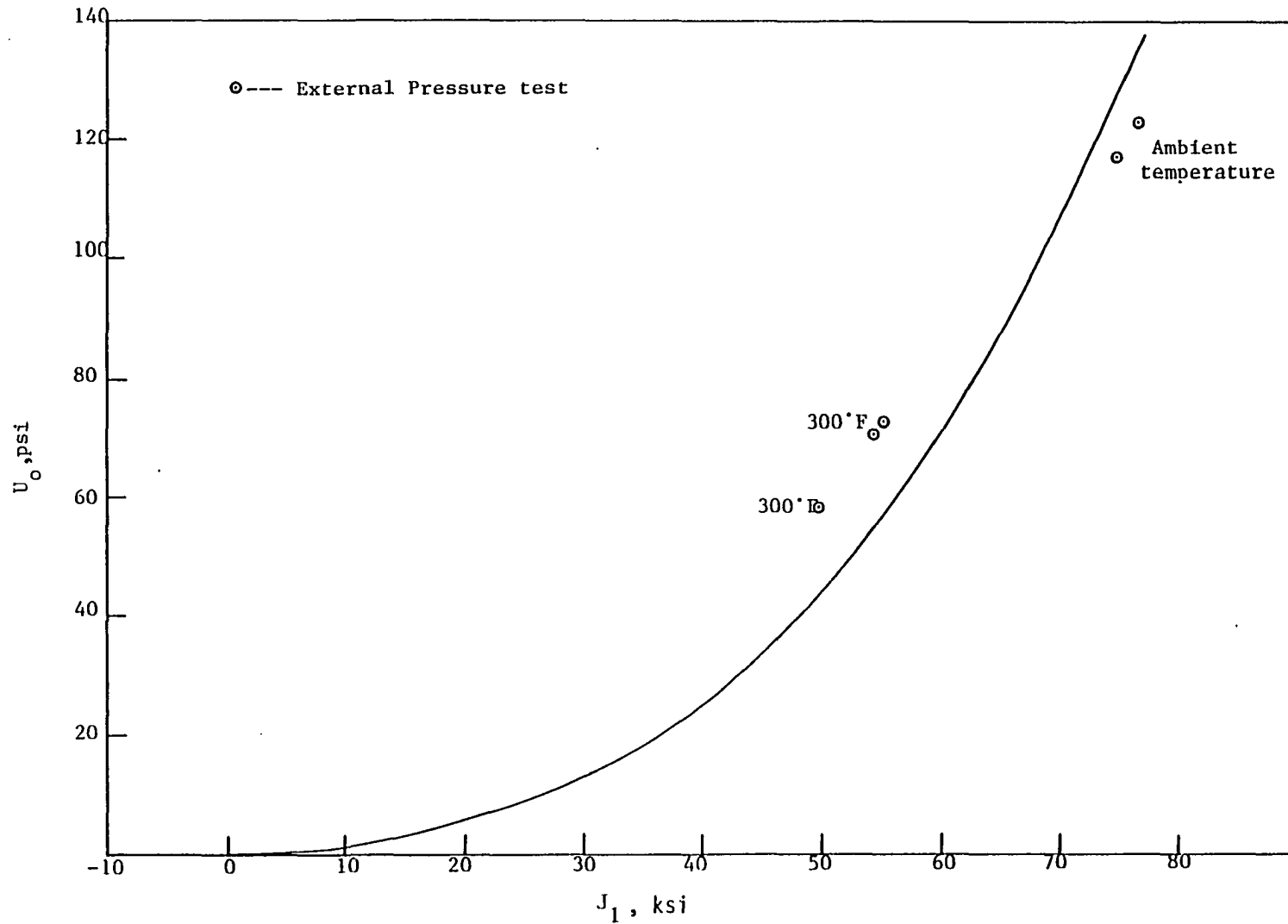


Figure 25. A plot of U_0 versus J_1 showing the external pressure test results at ambient temperature and at 300°F along with a plot of equation (14).

4c. Comparison with Previous Fracture Data on Granite at Ambient Temperature and at High Temperature

Experimental results of three independent investigators (Wong (46), Brace et al. (45), and Smith et al. (21)) who have performed failure tests on granite under different pressures and at various temperatures were selected, and their experimental results were compared with the existing criteria of Coulomb-Mohr, Drucker-Prager and our new proposed criterion in terms of U_0 and J_1 . Wong (46) has thoroughly investigated the failure of Westerly granite at pressures of up to 58 ksi (400 MPa) and temperatures up to 1290° F (700° C). Experimental investigation on the volume change of granite under triaxial compression at confining pressure of as much as 110 ksi (8Kbar) was carried out by Brace et al. (45). Failure data of granite under triaxial compression have also been reported by Smith et al. in their experiments the rocks were tested at confining pressures as high as 90 ksi. The experimental results of these three investigators are plotted in terms of $\frac{\sigma_1 + \sigma_3}{2}$ versus $\frac{\sigma_1 - \sigma_3}{2}$, J_1 versus $\sqrt{J_{2d}}$ and J_1 versus U_0 in Figures 26, 27, and 28 respectively.

Observing the plot of these experimental values in Figure 26 and comparing it with equation (2), which represents the Coulomb-Mohr criterion, a wide scatter is observed between the predicted and the experimental values. Similarly observing the same experimental data, but now in terms of J_1 and $\sqrt{J_{2d}}$ and comparing it with equation (4), which represents the Drucker and Prager criterion an equal amount of scatter is observed between the predicted and the experimental values. From the plots in Figures 26 and 27, it is also observed that for different values of pressure, Wong's results fell on different straight lines. In order to demonstrate the effectiveness of the new proposed criterion [in terms of U_0 and J_1 as given by equation (14)] over that of Coulomb-Mohr and Drucker and Prager criteria the same experimental

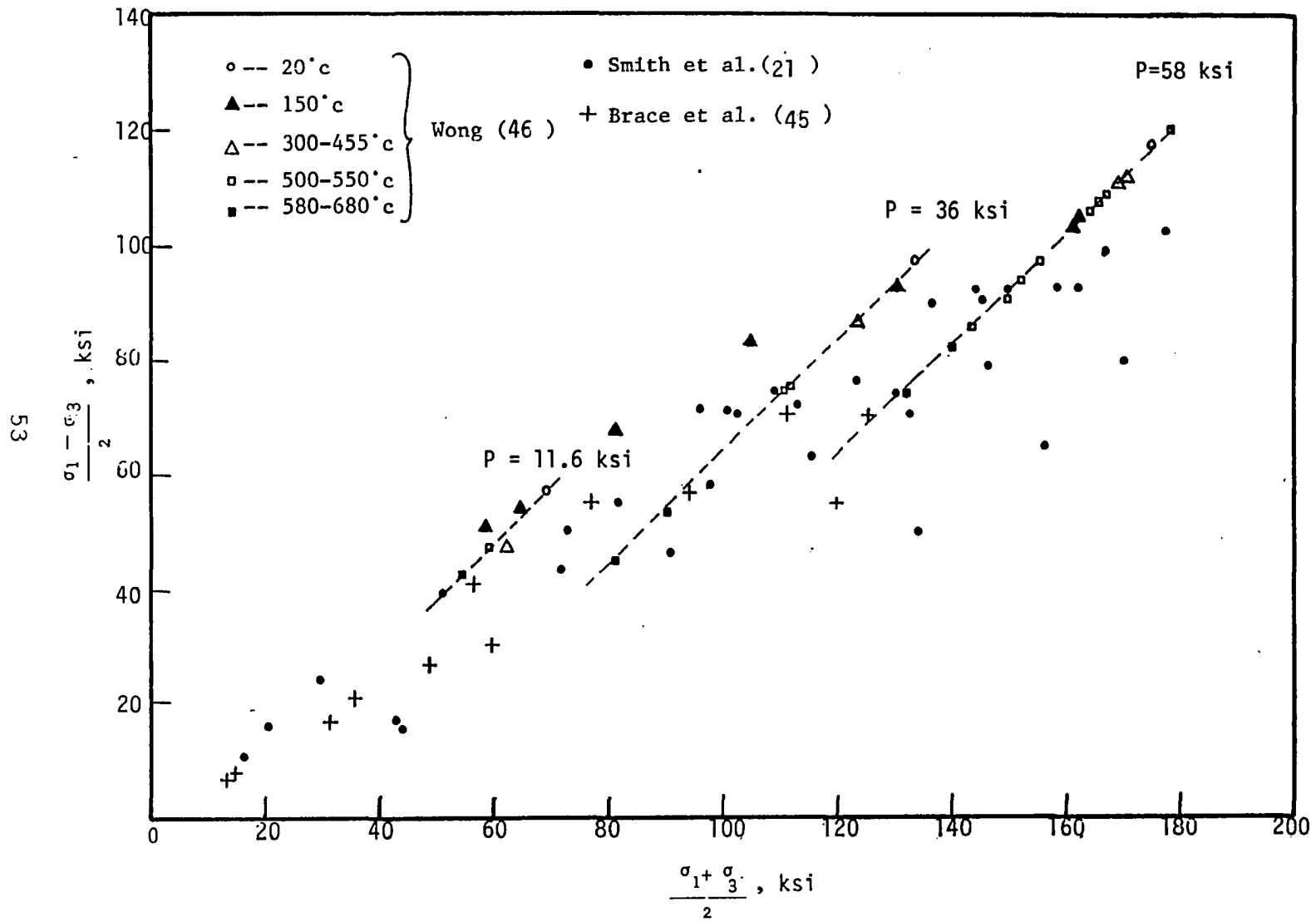


Figure 26. A plot of $\frac{\sigma_1 - \sigma_3}{2}$ versus $\frac{\sigma_1 + \sigma_3}{2}$

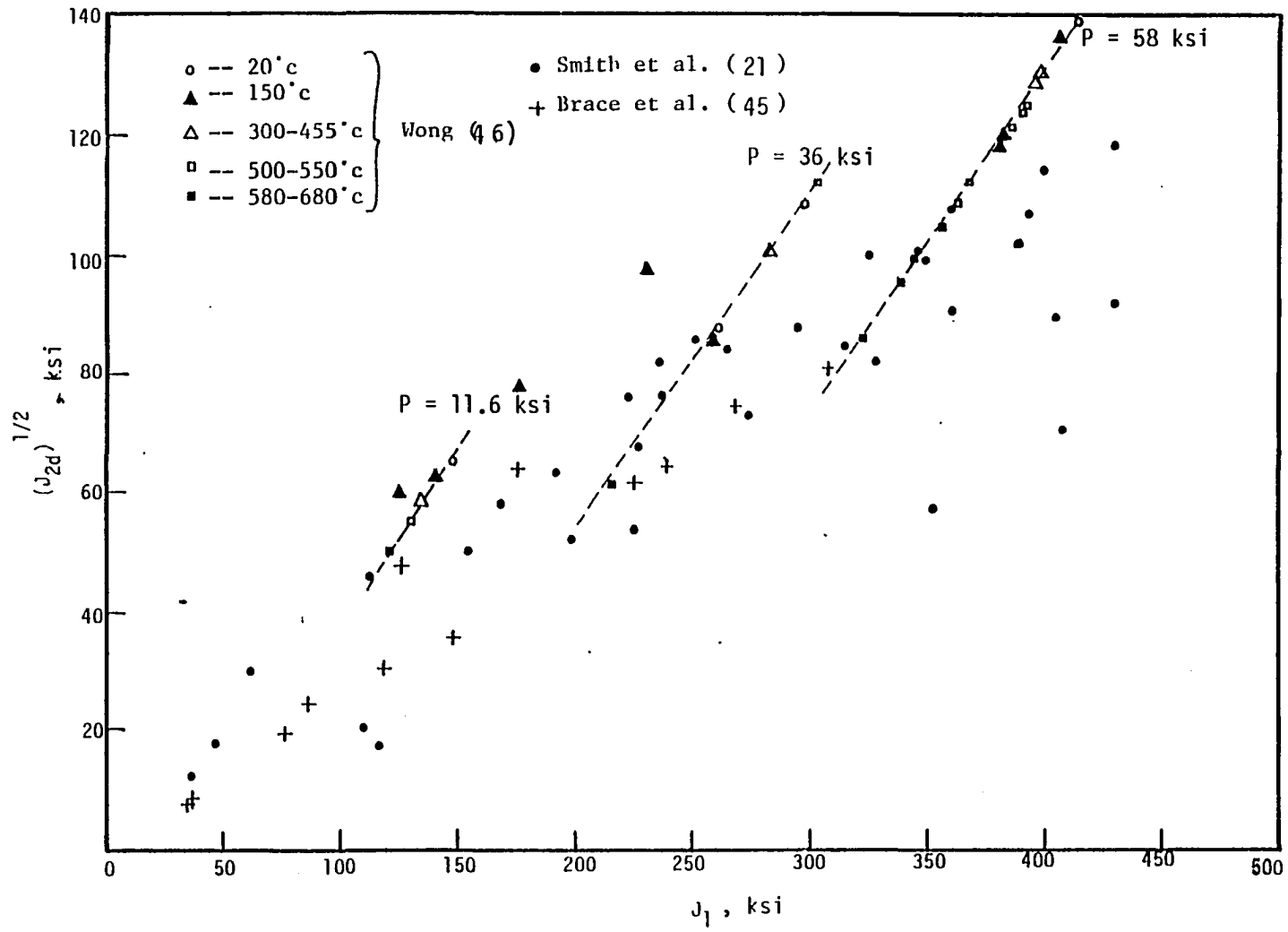


Figure 27. A plot of $(J_{2d})^{1/2}$ versus J_1 .

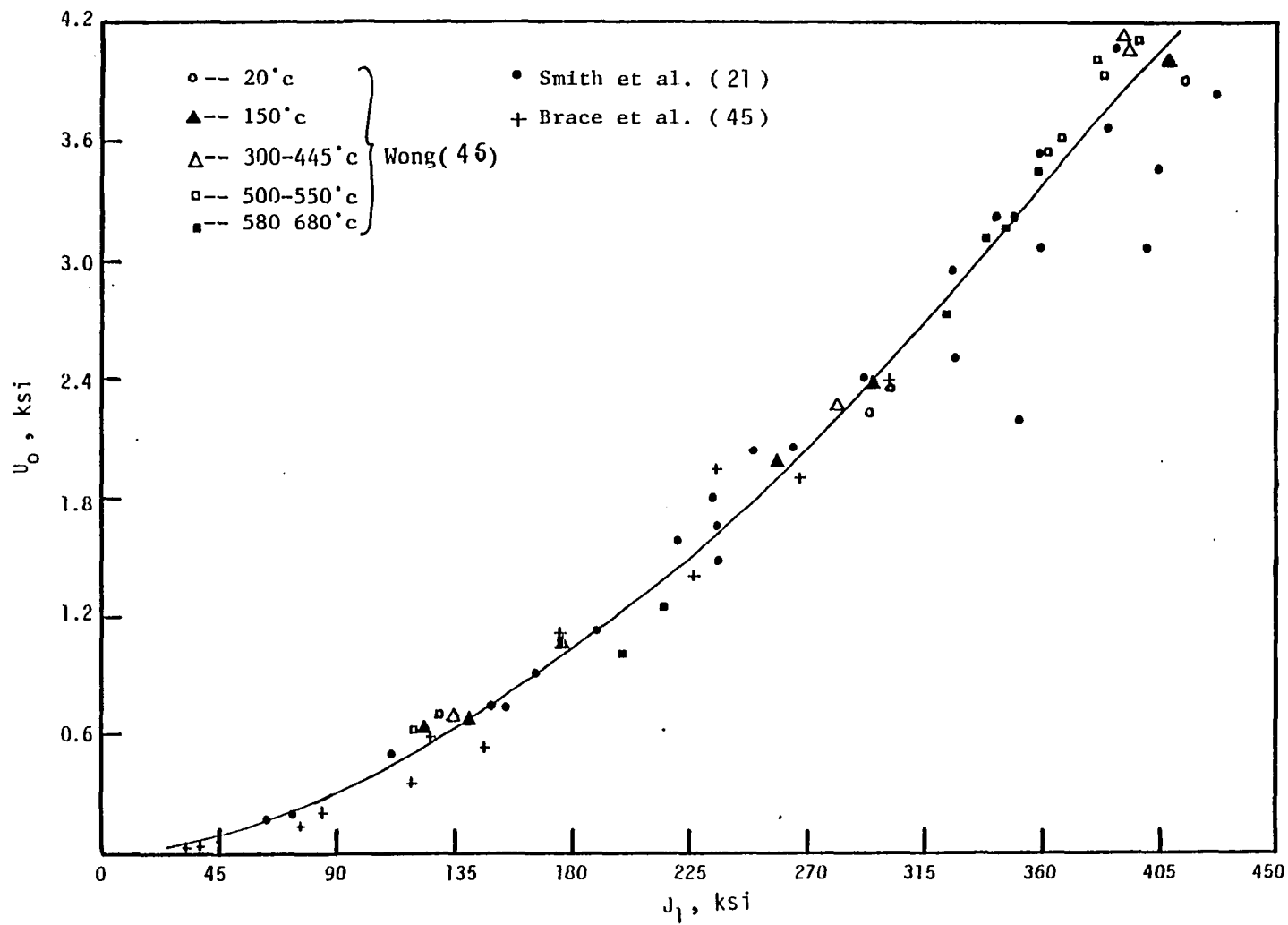


Figure 28 . A plot of U_0 versus J_1 .

data are plotted in terms of U_0 and J_1 and compared with equation (14) in Figure 28. A very minimal scatter is observed between the experimental results and the values predicted by equation (14). The constants evaluated by using the least square fit program in this case are given by

$$\alpha = 1.07 \text{ psi}$$

$$\theta = 19 \times 10^{-5}$$

$$\tau = 3.711 \times 10^{-8} \text{ psi}^{-1}$$

$$\beta = 3 \times 10^{-16} \text{ psi}^{-2}$$

Also, the preliminary conclusion that the material parameters α , θ , τ , and β are independent of temperature is further confirmed when the experimental data of Wong (45) (Figure 28), which ranged from ambient temperature to as high as 1300° F), is observed to fall on the same curve. Thus it has been demonstrated that the proposed failure criterion in terms of U_0 and J_1 as given by equation (14) is very effective in predicting the failure behavior of granite not only under a wide range of stress values but also at various temperatures.

4d. Comparison of the Fracture Criteria with the Failure Results of Four Commonly Studied Rocks

In the previous section it was successfully demonstrated that the proposed new criterion in terms of U_0 and J_1 was relatively more effective in predicting the failure behavior of granite for the experimental results of three independent investigators. In this section, the failure results of four commonly studied rocks, (Solenhofen Limestone, sandstone, marble and shale) will be compared with the failure criteria of Coulomb-Mohr, Drucker and Prager, and the proposed new criterion.

The failure behavior of Solenhofen Limestone has been extensively studied

by many investigators in the past. The experimental results of Heard, Handin, Robertson, Serdengecti and Boozer⁽³⁶⁾, and Green et al.⁽¹⁸⁾, for the failure of Solenhofen limestone are compared with the three failure criteria. Figures 29, 30 and 31 show the plot of $\frac{\sigma_1 + \sigma_3}{2}$ versus $\frac{\sigma_1 - \sigma_3}{2}$, J_1 versus $\sqrt{J_2d}$ and J_1 versus U_0 respectively, which represent the Coulomb-Mohr, Drucker and Prager, and the proposed new criterion respectively. Observing the plots of these three failure criteria with the experimental results in Figures 29, 30 and 31 one sees a wide scatter between the experimental results and the predicted values using Coulomb-Mohr and Drucker and Prager (Figures 29 and 30). The scatter band is considerably narrowed when the same experimental data are plotted in terms of the proposed new criterion in terms of J_1 and U_0 . Thus, once again, the improved effectiveness of the proposed new criterion in predicting the failure of Solenhofen limestone relative to the other two criteria is demonstrated. The failure behavior of the other three commonly studied rocks (sandstone, marble, and shale) has been extensively investigated by Smith et al. ⁽²¹⁾. The failure results of these three rocks are also compared with failure criteria of Coulomb-Mohr, Drucker and Prager, and the proposed new criterion. The plots of these three failure criteria along with the experimental results of sandstone, marble, and shale are plotted in Figures 32, 33, and 34 respectively. Observing the plots in Figures 32, 33, and 34, one concludes that the failure of sandstone, marble, and shale can be equally effectively predicted by failure criteria of Coulomb-Mohr, Drucker and Prager, and the proposed new criterion.

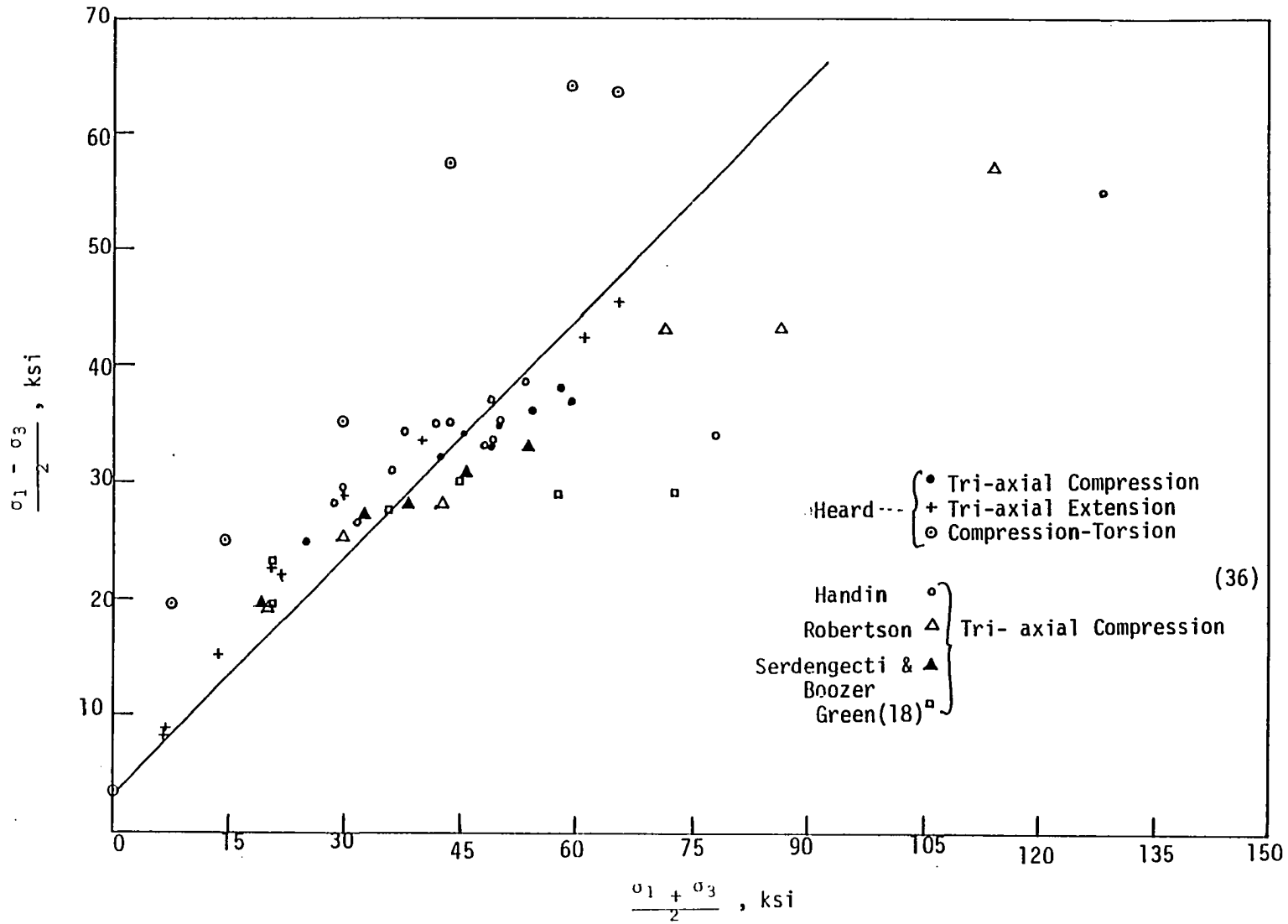


Figure 29. A plot of $\frac{\sigma_1 - \sigma_3}{2}$ versus $\frac{\sigma_1 + \sigma_3}{2}$ for Solenhofen Limestone

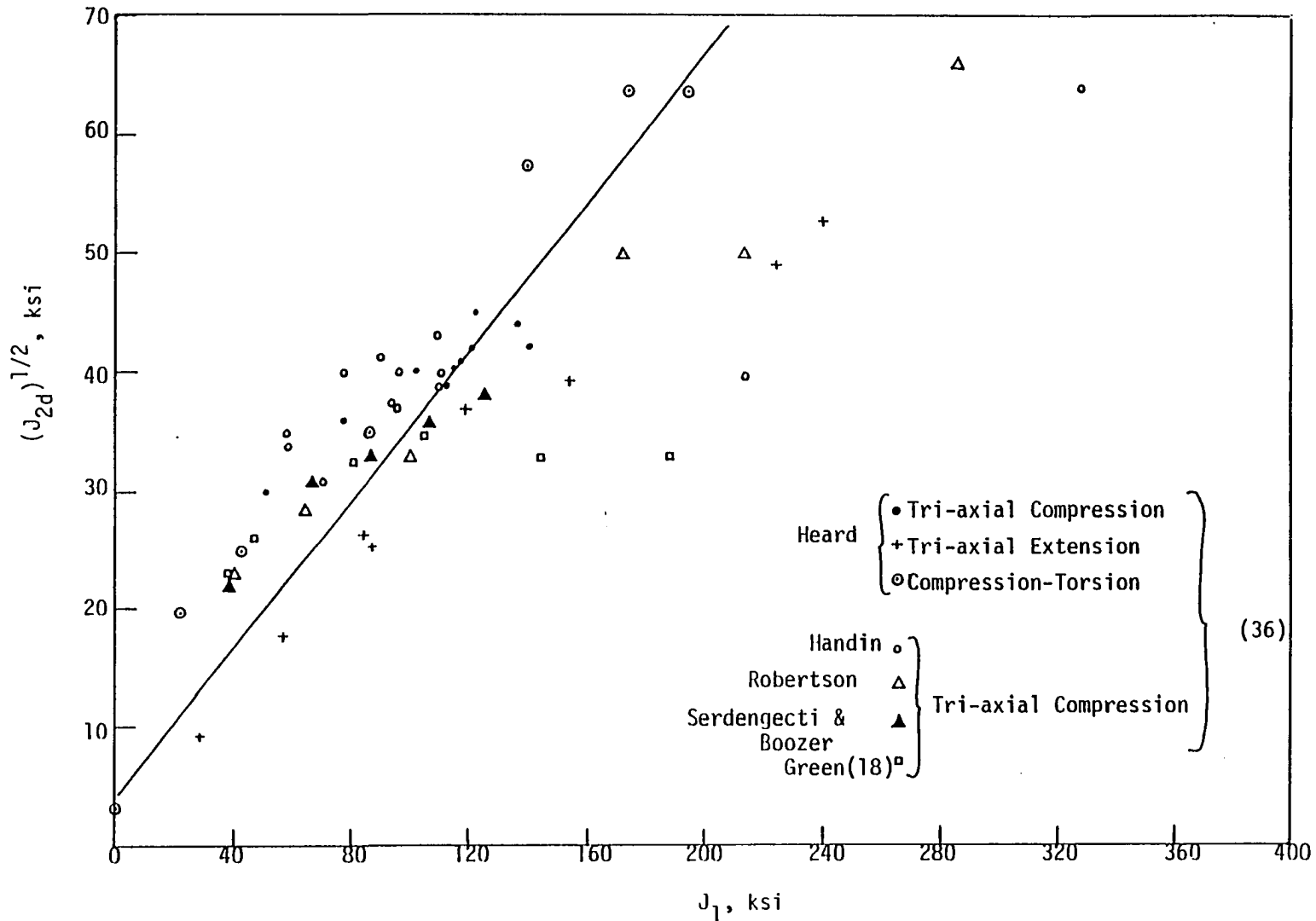


Figure 30. A plot of $(J_{2d})^{1/2}$ versus J_1 for Solenhofen Limestone

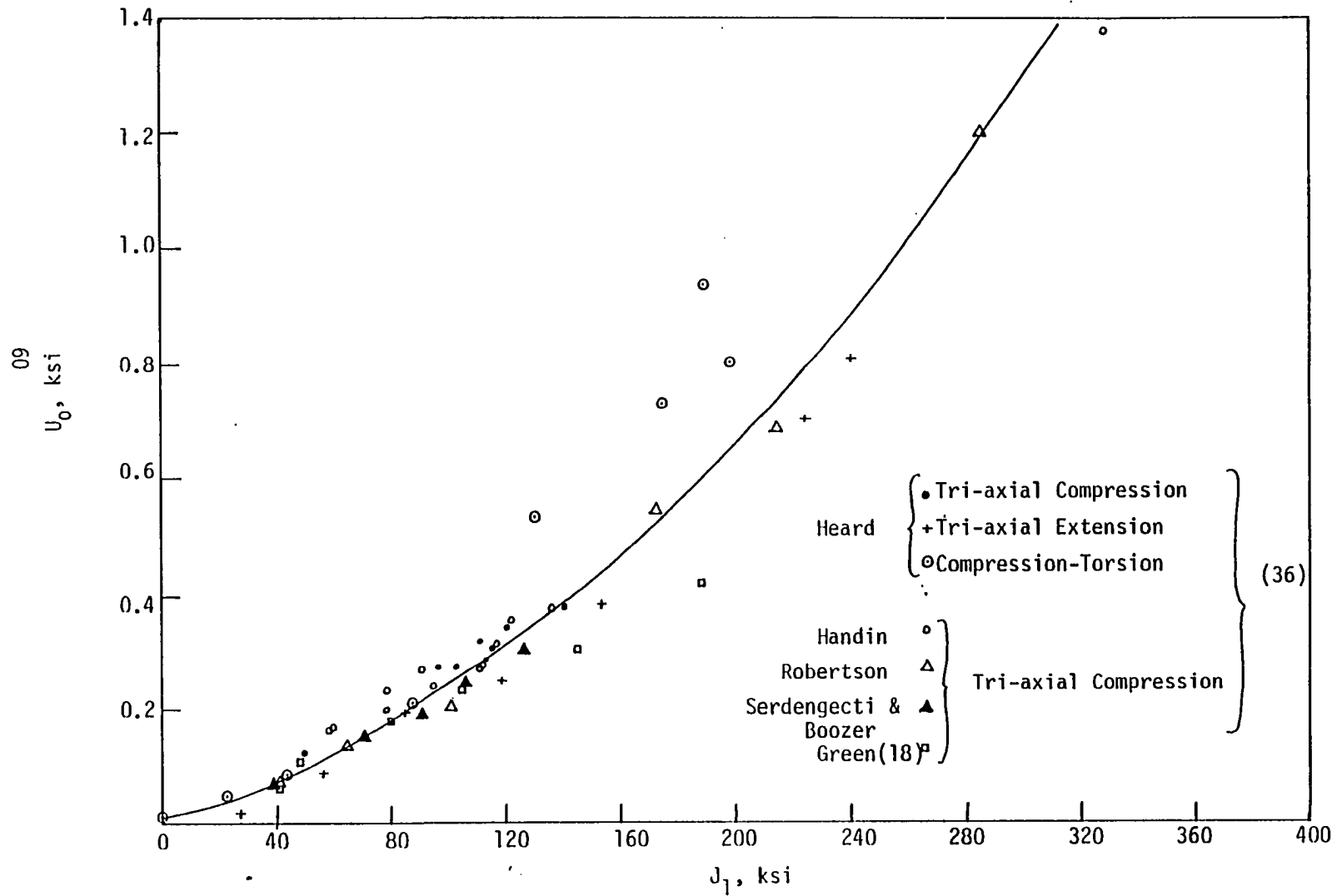


Figure 31. A plot of U_0 versus J_1 for Solenhofen Limestone.

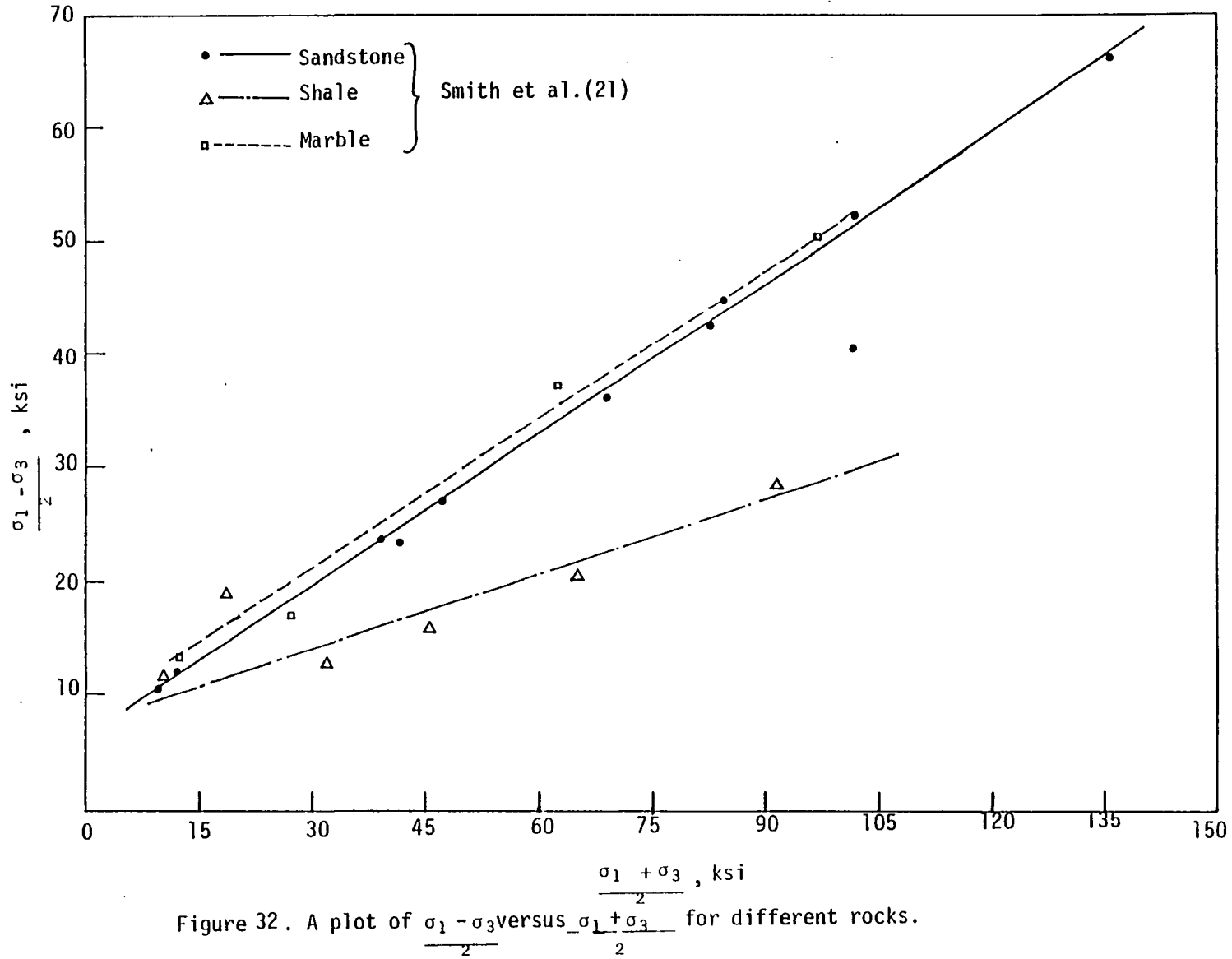


Figure 32. A plot of $\sigma_1 - \sigma_3$ versus $\frac{\sigma_1 + \sigma_3}{2}$ for different rocks.

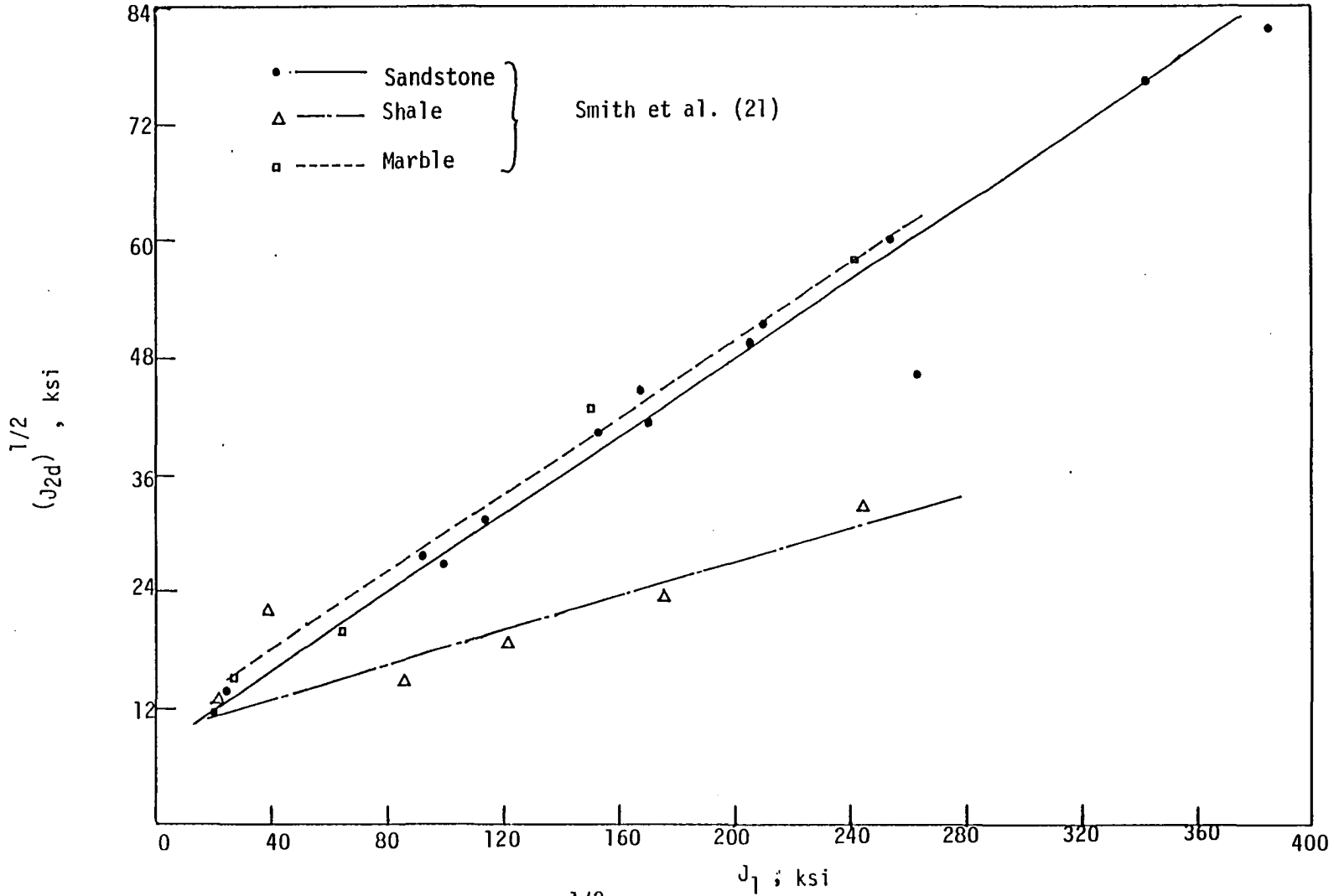


Figure 33. A plot of $(J_{2d})^{1/2}$ versus J_1 for different rocks.

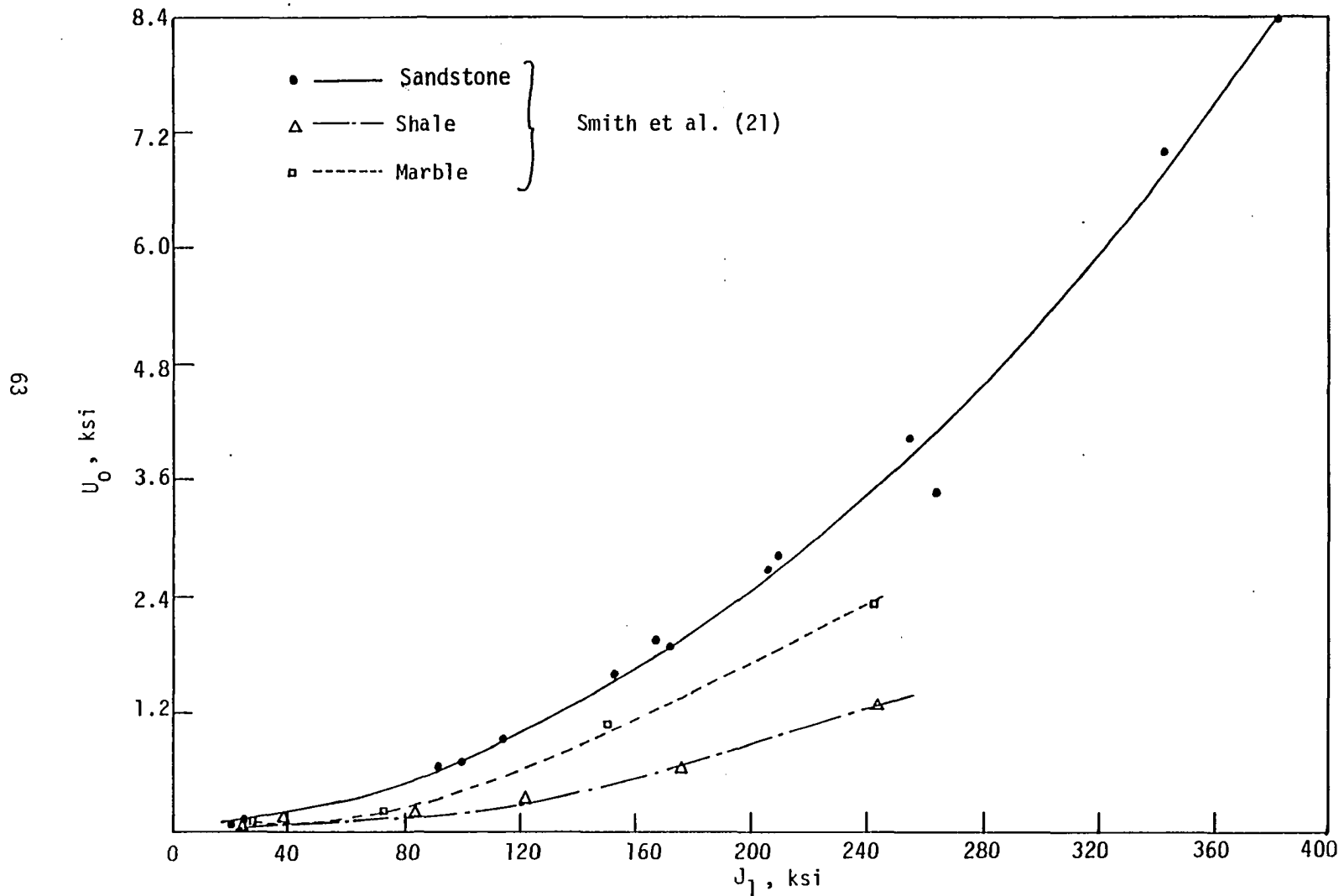


Figure 34 . A plot of U_0 versus J_1 for different rocks.

5. SUMMARY AND CONCLUSION

An experimental apparatus has been developed to study the behavior of rocks until failure under truly three dimensional loading. In these experiments, stress components are prescribed and the resulting strains are accurately measured by bonded strain gage rosettes on the surface of the core. The two loads, tension/compression and torsion, are applied independently of each other and also the corresponding strains are measured independently of each other. All the experiments were carried out on thin walled hollow cores, and therefore, the assumption of uniform shear stress or stresses due to pressure through the thickness is more appropriate than in the case of solid or thick walled cores.

The experimental results are compared with the failure criteria of Tresca, Coulomb-Mohr, von Mises, and Drucker and Prager. It is shown that none of these failure criteria are able to predict the failure behavior over the entire range of stress values. A new failure criterion, which incorporates bimodular rock behavior, is developed in terms of strain energy density U_0 and the first invariant of stress tensor J_1 and is given by equation (14). It has also been shown that this new failure criterion is able to predict the failure behavior over the entire range of stress values at failure including extremely high values of J_1 , and is also able to predict the failure behavior of granite at different temperatures.

The experimental results of three independent investigators are compared with the failure criterion of Coulomb-Mohr, Drucker and Prager and our new proposed criterion given by equation (14) in Figures 26, 27, and 28 respectively. Observing the plot in Figures 26, 27, and 28, one can conclude that the proposed new failure criterion is more effective in predicting the failure of granite than the Drucker and Prager and Coulomb-Mohr criteria.

Lastly, the failure results of four commonly studied rocks (Solenhofen Limestone, sandstone, marble, and shale) are compared with the failure criteria of Coulomb-Mohr, Drucker and Prager, and the proposed new criterion. In the case of Solenhofen limestone, the proposed new criterion was shown to be more effective in predicting the failure of limestone over the other two criteria. But, in the case of sandstone, shale, and marble, all the three failure criteria were shown to be equally effective.

REFERENCES

- 1) F. D. Adams and J. T. Nicholson, "An Experimental Investigation into the Flow of Marble," *Phil. Trans. Roy. Soc. London, Ser. A*, Vol. CXCIV (1901), pp. 363-401.
- 2) F. D. Adams and E. G. Coker, "Flow of Marble," *Amer. Jour. Sci.*, Vol. XXIX (4th Ser., 1910), pp. 465-85.
- 3) F. D. Adams, "An Experimental Investigation into the Action of Differential Pressure on Certain Minerals and Rocks, Employing the Process Suggested by Professor Kick," *Jour. Geol.*, Vol. XVII (1910), pp. 489-525. "An Experimental Contribution to the Question of the Depth of Zone on the Flow in the Earth's Crust," *ibid.*, Vol. XX (1912), pp. 97-118.
- 4) F. D. Adams and J. A. Bancroft, "Internal Friction during Deformation and the Relative Plasticity of Different Types of Rocks," *Jour. Geol.*, Vol. XXV (1917), pp. 597-637.
- 5) Th. Von Karman, "Festigkeitversuche unter allseitigem druck," *Zeitschr. des Vereins deutscher Ingenieure*, Vol. LV (1911) pp. 1749-57. For a discussion of this paper see W. H. Bucher, "The Mechanical Interpretation of Joints," *Jour. Geol.*, Vol. XXIX (1921), p. 13.
- 6) P. W. Bridgman, *The Physics of High Pressure* (New York: Macmillan Co., (1931), chap. II and III.
- 7) D. Griggs, and W. B. Miller, "Deformation of Yule Marble: Part I: Compression and Extension Experiments on Dry Yule Marble at 10,000 Atmosphere Confining Pressure, Room Temp," *Bull. of the Geol. Soc. of America*, vol. 62, (Aug. 1951), pp. 853-862.
- 8) D. Griggs, "Experimental Flow of Rocks," *Bull. Geol. Soc. America*, Vol. 51, (1940), pp. 1002-1033.
- 9) D. T. Griggs, "Deformation of Rocks Under High Confining Pressures. I. Experiments at Room Temperature," *Jour. of Geol.*, Vol. XLIV, #5, (1936), pp. 541-577.
- 10) D. T. Griggs, "Creep of Rocks," *Jour. of Geol.*, Vol. XLVIII, #3, (1939), pp. 225-251.
- 11) D. C. Drucker and W. Prager, "Soil Mechanics and Plastic Analysis of Limit Design," *Quart. Appl. Math.*, Vol. 10, No. 2, (1952), pp. 157-165.
- 12) D. T. Griggs and J. Handin, eds., *Rock Deformation*, *Geol. Soc. Amer. Memoir 79* (1960).
- 13) A. Leith and J. A. Sharpe, "Deep-focus Earthquakes and their Geological Significance," *Jour. Geol.*, Vol. 44, No. 8, (1936), p. 877-917.

- 14) E. C. Robertson, "Experimental Study of the Strength of Rocks", Bull. of the Geo. Soc. of Am., Vol. 66, (Oct. 1955), pp. 1275-1314.
- 15) F. J. Turner, D. T. Griggs, R. H. Clark, and R. H. Dixon, "Deformation of Yule Marble. Part VII: Development of Oriented Fabrics at 300°C-500°C," Bull. Geol. Soc. Amer., Vol. 67, (1956), pp. 1259-1294.
- 16) D. T. Griggs, F. J. Turner, and H. C. Heard, 1960, "Deformation of Rocks at 500° to 800°C," Geol. Soc. Amer. Memoir 79, pp. 39-104.
- 17) E. H. Rutter, "The Effects of Strain-Rate Changes on the Strength and Ductility of Solenhofen Limestone at Low Temperatures and Confining Pressures," Int. Jr. of Rock Mec. and Min. Sci., Vol. 9, No. 2, (March 1972), pp. 183-189 .
- 18) S. J. Green, et al., "Triaxial Behavior of Solenhofen Limestone and Westerly Granite at High Strain Rates," Jr. of Geophysical Research, Vol. 77, No. 20, (July 1972), pp. 3711-3724.
- 19) S. Serdengecti, and G.D. Bozer, "The Effects of Strain Rate and Temperature on the Behavior of Rocks Subjected to Triaxial Compression," in Fourth Symposium on Rock Mechanics, Pennsylvania State University, University Park, (1961), pp. 83-97.
- 20) A.M. Price and I.W. Farmer, "A General Failure Criterion for Rocks" Proceedings of the 21st U.S. Symp. on Rock Mechanics, (May 1980), pp. 256-263.
- 21) J.L. Smith, K.L. DeVries, D.J. Bushnell and W.S. Brown, "Fracture Data and Stress-Strain Behavior of Rocks in Triaxial Compression," Experimental Mechanics, Vol. 8, No. 8, (Aug. 1969), pp. 348-355.
- 22) M.R.H. Ramez, "Fracture and the Strength of Sandstone Under Triaxial Compression," Int. J. of Rock Mech. and Min. Sci., Vol. 4, (1967), pp. 257-268,
- 23) T. W. Miller, and J. B. Cheatham, Jr., "A New Yield Condition and Hardening Rule for Rocks." Int. Jr. of Rock Mech. and Min. Sci., Vol. 9, No. 4, (July 1972), pp. 453-474.
- 24) A. Kumar, "The Effect of Stress Rate and Temperature on the Strength of Basalt and Granite," Geophysics, Vol. 33, (1968), pp. 501.
- 25) W. Goldsmith, J.L. Sackman, and C. Ewerts, "Static and Dynamic Fracture Strength of Barre Granite," Int. J. of Rock Mech. Min. Sci. and Geomech. Abstr. Vol. 13, (1976), pp. 303-309.
- 26) Nur, A., and Byerlee, J.D., "An Exact Effective Stress Law for Elastic Deformation of Rock with Fluids," Jr. of Geophysical Research Vol. 76, No. 26, (Sept. 1971), pp. 6414-6419.
- 27) G. Barla, "Some Constitutive Equations for Rock Materials," Proceedings, Eleventh Symposium on Rock Mechanics, University of California, Berkeley, (June 1969), pp. 221-236.

- 28) S. K. Bordia, "Complete Stress-Volumetric Strain Equation for Brittle Rock up to Strength Failure," *Int. Jr. of Rock Mech. and Min. Sci.*, Vol. 9, No. 1, (Jan. 1972), pp. 17-24.
- 29) J.A. Hudson, E. T. Brown, and C. Fairhurst, "Shape of the Complete Stress-Strain Curve for Rock," *Proceedings, Thirteenth Symposium on Rock Mechanics*, (Aug. 1971), pp. 773-795.
- 30) W.R. Judd and C. Huber, "Correlation of Rock Properties by Statistical Methods," *Proc. Int. Sym. on Mining Research, held at University of Missouri, Rolla, Vol. 2*, (Feb. 1961), pp. 621-649.
- 31) F. E. Heuze, "High Temperature Mechanical, Physical and Thermal Properties of Granite Rocks," *Int. Jr. of Rock Mec. and Min. Sci. and Geomech. Abstr. Vol. 20, No. 1*, (1983), pp. 3-10.
- 32) D.W. Hobbs, "Tensile Strength of Rocks," *Int. J. of Rock Mech. and Min. Sci. Vol. 1*, (1964), pp. 385-396.
- 33) A. W. Khair and H.R. Hardy Jr., "Failure of Indiana Limestone Under a Tension-Tension Compression Stress State," *Energy Resources and Excavation Technology, Proceedings, Eighteenth U.S. Symposium on Rock Mechanics*, (June 1977), pp. 381-1-381-9.
- 34) R. E. Ely, "Strength of Graphite Tube Specimens Under Combined Stresses," *J. of American Ceramic Society, Vol. 48, No. 10*, (Oct. 1965), pp. 505-508.
- 35) B. Paul, "A Modification of the Coulomb Mohr Theory of Fracture," *Jr. of Appl. Mech.*, Vol. 28, No. 2, (June 1961), pp. 259-268.
- 36) J. Handin, H.C. Heard, and J.N. Magourik, "Effect of the Intermediate Principal Stress on the Failure of Limestone, Dolomite and Glass at Different Temperatures and Strain Rates," *Jr. of Geophysical Research, Vol. 72, No. 2*, 1967, pp. 611-640.
- 37) S. R. Swanson and W. S. Brown, "The Influence of State of Stress on the Stress-Strain Behavior of Rocks," *Jr. of Basic Engineering, Transactions of the ASME, Series D, Vol. 94, No. 1*, pp. 238-242, May 1972.
- 38) W. Van Der Knapp, "Nonlinear Behavior of Elastic Porous Media," *Trans. AIME, Petroleum Branch, Vol. 216*, pp. 179-187, 1959.
- 39) N. Cristescu, "Rock Dilatometry in Uniaxial Tests," *Rock Mech.*, Vol. 15, No. 3, (Nov. 1982), p. 133-144.
- 40) M.K. Kim, and P.V. Lade, "Modelling Rock Strength in Three Dimensions," *Int. J. of Rock Mech. and Min. Sci. and Geomech. Abstr.*, Vol. 21, No. 1, (1984), pp. 21-33.
- 41) D. C. Drucker, "Limit Analysis of Two and Three-dimensional soil mechanics problems." *J. Mech. Phys. Solids, Vol. 1*, (1953), pp. 217-226.

- 42) H. Kupfer, H.K. Hilsdorf, and H. Rusch, "Behavior of Concrete under biaxial stress," J. Am. Concrete Inst., Proc., Vol. 66, No. 8, (1969), pp. 656-666.
- 43) Vile, G.W.D., "The Strength of Concrete under the Short-term Static Biaxial Stress," In: A.E. Brooks and K. Newman (Editors), The Structure of Concrete and its Behavior under Load, (1968).
- 44) W. F. Chen, Limit Analysis of Soil Plasticity, Elsevier Scientific Publishing Company, New York, (1975).
- 45) W. F. Brace, B. W. Paulding, Jr., and C. Scholz, "Dilatancy in the fracture of crystalline rocks," J. of Geophysical Research Vol. 71, No. 16, (Aug. 1966), pp. 3939-3953.
- 46) T. F. Wong, "Effects of Temperature and Pressure on the Failure and Post-failure Behavior of Westerly granite," Mechanics of Materials Vol. 1, No. 1, (Jan. 1982), pp. 3-17.
- 47) T. F. Wong, "Shear Fracture Energy of Westerly Granite from Post Failure Behavior," J. Geophysical Res. Vol. 87, No. 10, (Feb. 1982), pp. 990-1000.
- 48) S. A. Ambartsumyan and A. A. Khachatryan, "Basic Equation of the Theory of Elasticity for Materials with Different Resistance to Tension and Compression," Mekhanika Tverdogo Tela, Vol. 1, (1966), p. 44.
- 49) R. C. Novak and C. W. Bert, "Experimental and Theoretical Bases for Determination of More Precise Properties of Epoxy," Jour. of Composite Materials, Vol. 2, (Oct. 1968), pp. 506-508.
- 50) J. E. Russel and E. R. Hoskins, "Residual Stresses in Rocks," Proceedings, Fourteenth Symposium on Rock Mechanics, (June 1972), pp. 1-23.

APPENDIX

TABLE 5

Experimental Data of Wong (46), for Westerly Granite

Sp. No.	σ_1 ksi	σ_2 ksi	σ_3 ksi	Temp. °C	E x 10 ⁶ psi	U ₀ ksi
PFW26	126	11.6	11.6	20	10.4	0.731
PFW22	118.9	11.6	11.6	150	9.46	0.693
PFW23	113.1	11.6	11.6	350	8.47	0.697
PFW28	107.3	11.6	11.6	551	7.49	0.7
PFW30	97.17	11.6	11.6	659	6.95	0.62
HTW53	110.2	7.25	7.25	151	9.46	0.61
HTW52	147.9	14.5	14.5	151	9.46	1.07
HTW51	188.5	21.75	21.75	151	9.46	1.72
MTW8	128.18	36.26	36.26	668	6.93	1.0
MTW9	143.58	36.26	36.26	611	7.2	1.25
MTW7	185.6	36.26	36.26	551	7.49	2.03
MTW5	187.1	36.26	36.26	455	7.9	1.96
MTW4	210.29	36.26	36.26	302	8.72	2.25
MTW1	223.35	36.26	36.26	155	9.4	2.37
MTW11	230.6	36.26	36.26	20	10.1	2.36
MTW12	223.35	36.26	36.26	20	10.1	3.21
HTW54	298.76	58	58	20	10.1	3.9
HTW50	292.96	58	58	154	9.46	4.00
HTW49	279.9	58	58	352	8.47	4.07
HTW43	281.36	58	58	353	8.47	4.11
HTW33	269.76	58	58	426	8.1	3.94
HTW46	265.4	58	58	503	7.74	3.99
HTW0	246.55	58	58	550	7.49	3.54
HTW45	229.15	58	58	611	7.2	3.17
HTW28	207.3	58	58	680	6.85	2.73
HTW36	275.56	58	58	425	8.1	4.12
HTW47	274.11	58	58	422	8.1	4.07
HTW35	266.86	58	58	499	7.7	4.06
HTW30	252.36	58	58	507	7.74	3.6
HTW44	240.75	58	58	580	7.35	3.44
HTW27	223.35	58	58	660	6.95	3.12

TABLE 6

Experimental Data of Brace (45) [$E = 7.25 \times 10^6$ psi, $\nu = 0.2$]
For Granite at Ambient Temperature

σ_1 ksi	σ_2 ksi	σ_3 ksi	U_o ksi
20.3	7.25	7.25	0.0264
21.75	7.395	7.395	0.03
47.85	14.5	14.5	0.144
56.55	14.5	14.5	0.207
75.4	21.75	21.75	0.354
90.625	29	29	0.514
175.45	63.8	63.8	1.954
195.75	55.1	55.1	2.38
175.45	46.4	46.4	1.911
150.8	37.7	37.7	1.411
131.95	21.75	21.75	1.095
97.15	14.79	14.79	0.596

TABLE 7

Experimental Data of Smith (21) for Granite ($E = 7.5 \times 10^6$, $\nu = 0.2$)

Run No.	σ_1 ksi	σ_2 ksi	σ_3 ksi	U_0 ksi
100	167	35	35	1.678
101	136.7	27	27	1.126
103	53.4	5	5	0.178
104	110	23	23	0.728
105	162.2	30	30	1.59
106	90.4	11	11	0.504
108	183	34	34	2.02
109	123	23	23	0.914
110	185	40	40	2.057
111	172.9	31	31	1.8
200	204	62	62	2.5
201	265.5	67.5	67.5	4.23
202	280	75	75	4.7
203	200	47	47	3.4
204	232	56	56	3.23
205	222.6	51.6	51.6	2.975
206	243	58	58	3.54
207	230.5	59.5	59.5	3.188
209	246.4	70	70	3.65
210	157	40	40	1.479
211	254.8	69	69	4.07
300	184	84	84	2.18
301	238.5	83.5	83.5	3.47
302	225.5	67.5	67.5	3.06
303	221	91	91	3.06
304	250	90	90	3.83
400	137.3	44	44	1.14
401	58.8	28.8	28.8	0.228
402	26.5	5.5	5.5	0.0425
403	36	5	5	0.0794
404	60	25	25	0.226
405	178.5	52.5	52.5	1.918
406	204	56	56	2.499

TABLE 8

Experimental Data of Smith et al. (21) for Sandstone
 [E = 2.44×10^6 psi, $\nu = 0.25$]

Run No.	σ_1 ksi	σ_2 ksi	σ_3 ksi	U_0 ksi
1	20.37	-	-	0.085
2	97.5	27.5	27.5	1.63
3	129.1	40	40	2.84
4	64.5	18	18	0.71
5	105	33	33	1.88
6	24	-	-	0.118
20	141.12	61	61	3.46
21	62.5	15	15	0.678
22	154	50	50	4.05
24	107.5	30	30	1.98
25	125	40	40	2.67
26	74	20	20	0.942
27	222.36	81	81	8.46
28	202	70	70	6.97

TABLE 9

Experimental Data of Smith et al. (21) for Marble
[$E = 3.82 \times 10^6$ psi, $\nu = 0.25$]

Run No.	σ_1 ksi	σ_2 ksi	σ_3 ksi	U_0 ksi
501	147	47	47	2.36
502	99	25	25	1.08
503	44	10	10	0.215
500	25.8	-	-	0.087

TABLE 10

Experimental Data of Smith et al. (21) for Shale
[$E = 2.44 \times 10^6$ psi, $\nu = 0.25$]

Run No.	σ_1 ksi	σ_2 ksi	σ_3 ksi	U_o ksi
8	38.2	-	-	0.146
9	61.8	30	30	0.331
10	22.3	-	-	0.05
11	45.4	20	20	0.175
12	86	45	45	0.656
13	119.8	62.5	62.5	1.27

TABLE 11

Experimental Data of Green et al. (18) for Solenhofen Limestone
 [E = 10.2×10^6 psi, $\nu = 0.25$]

σ_1 ksi	σ_2 ksi	σ_3 ksi	U_0 ksi
39.87	-	-	0.078
63.8	7.25	7.25	0.18
74.7	14.5	14.5	0.236
86.3	29	29	0.304
100.8	43.5	43.5	0.42
45.7	-	-	0.1

TABLE 12

Experimental data of Hendin et al. (36) for Solenhofen Limestone
 [E = 10.2×10^6 psi, $\nu = 0.25$]

Number	σ_1 ksi	σ_2 ksi	σ_3 ksi	U_0
183	58.43	5.075	5.075	0.1547
1184	74.38	10.005	10.005	0.242
1185	85.98	14.935	14.935	0.3158
1186	96.135	20.01	20.01	0.388
1278	67.425	5.075	5.075	0.208
1283	73.8	10.005	10.005	0.238
1277	81.63	14.935	14.935	0.283
144	50.31	-	-	0.124
28	79.895	11.02	11.02	0.278
24	85.26	14.935	14.935	0.31
116	82.07	14.935	14.935	0.286
115	91.35	18.415	18.415	0.351
27	95.7	22.185	22.185	0.381
1708	81.925	14.5	14.5	0.279
1712	112.52	43.5	43.5	0.52
1709	183.28	72.5	72.5	1.38
GT117	57.71	-	-	0.163
GT112	59.3	-	-	0.172
GT116	71.483	2.9	2.9	0.24
GT118	77.285	5.8	5.8	0.273
GT119	79.025	8.7	8.7	0.278
GT120	86.13	11.6	11.6	0.324
GT121	92.075	14.5	14.5	0.365
S99	39.875	-	-	0.078
S83	55.535	4.35	4.35	0.14
S86	71.05	14.21	14.21	0.21
S89	115.13	28.42	28.42	0.55
S87	129.34	42.65	42.65	0.683
S88	171.97	56.84	56.84	1.2
	39.44	-	-	0.0762
689	58.87	5.075	5.075	0.157
587	66.99	10.0	10.0	0.19
652	76.995	15.08	15.08	0.25
628	86.565	20.01	20.01	0.312
10	58.87	58.87	0.58	0.253
9	73.66	73.66	6.09	0.379
124	103	103	18.27	0.704
125	110.5	110.5	19.14	0.812
GT541	14.5	14.5	-1.6	0.022
GT542	14.5	14.5	-2.17	0.022
GT539	29	29	-1.74	0.085
GT540	29	29	-1.6	
GT543	43.5	43.5	-0.725	
GT544	43.5	43.5	-2.03	0.19

TABLE 12 (Cont.)

Number	σ_1 ksi	σ_2 ksi	σ_3 ksi	U_0
G-27,102				
112	3.335	0	-3.335	0.00136
G12	26.97	7.25	-12.47	0.051
G3	39.44	14.5	-10.44	0.091
G2	63.8	29	-5.8	0.21
G95	101	43.5	-14.06	0.54
G94	121.8	58	-5.8	0.746
G125	128.76	65.25	1.74	0.807
G32	143.5	43.5	1.45	0.94